The Thesis Committee for Apurva Sarathy

Certifies that this is the approved version of the following thesis:

AN IMMUNOHISTOCHEMICAL ANALYSIS OF REGENERATING CELLULAR MATERIAL IN TWO DISTINCT MODELS OF SKELETAL MUSCLE INJURY.

APPROVED BY

SUPERVISING COMMITTEE:

Supervisor: Roger Farrar

Laura Suggs

AN IMMUNOHISTOCHEMICAL ANALYSIS OF REGENERATING CELLULAR MATERIAL IN TWO DISTINCT MODELS OF SKELETAL MUSCLE INJURY.

by

Apurva Sarathy, B.S. Bio.

Thesis

Presented to the Faculty of the Graduate School of
The University of Texas at Austin
in Partial Fulfillment
of the Requirements
for the Degree of

Master of Science in Kinesiology

The University of Texas at Austin
August 2011

DEDICATION

This work is dedicated to my family and friends who have supported me in all my academic endeavors.

ACKNOWLEDGEMENTS

This work has been completed under the able guidance of my supervisor Dr. Roger Farrar whose mentorship was invaluable towards my academic progress. I am very grateful to Dr. Laura Suggs, who gave me the benefit of her academic experience, through her Tissue Engineering class, as well as graciously agreed to be my second reader. I would like to thank Patty Coffman for her tremendous assistance with administrative matters concerning the lab. Her willingness to help with administrative tasks ensured that all research in the lab was carried out smoothly. I'd like to thank all my former and current lab mates namely Ed Merritt, David Hammers, Matt Tierney, Megan Cannon, Rosemary French, Daria Neidre, Melissa Merscham, Tae Jong Song, Chantal Pham, Jessica Treff, Vika Rybalko and Adriana DaCosta. While some of my lab mates trained me in vital laboratory skills, others helped me tremendously in the completion of experimental protocols. They have all made my graduate school experience incredibly enjoyable.

AN IMMUNOHISTOCHEMICAL ANALYSIS OF REGENERATING CELLULAR MATERIAL IN TWO DISTINCT MODELS OF SKELETAL MUSCLE INJURY.

Apurva Sarathy, M.S. Kin.
The University of Texas at Austin, 2011
Supervisor: Roger P. Farrar

Tourniquet mediated Ischemia Reperfusion (I/R) injury causes damage to skeletal muscle, often resulting in prolonged functional impairment. The current study utilizes immunohistochemistry (IHC) to determine whether the controlled release of the anabolic factor, insulin-like growth factor-I (IGF-I), from the biodegradable PEGylated fibrin gel matrix can facilitate the recovery of skeletal muscle from I/R. Treatment groups following a 2-hour tourniquet applied to the limb of 6-9 month rats, included intramuscular injections of saline, PEGylated fibrin gel (PEG-Fib) only and IGF-I conjugated to PEGylated fibrin gel (PEG-Fib-IGF). Expression of the myogenic regulatory factors MyoD and myogenin detected via IHC in the PEG-Fib-IGF group was significantly lower compared to the saline group, showing a 1.4±0.8% nuclear co-localization for MyoD and a 2.0±0.8% nuclear co-localization for myogenin at 14 days of recovery. The saline group showed higher values, 31.4±4.4% and 44.1±7.3% for MyoD and myogenin nuclear co-localization respectively. A significantly greater percentage, 88.8±3.7% of Desmin positive myofibers was seen at 14 days of recovery, while a lower percentage of fibers expressing neonatal myosin, 7.7±2.7% was seen in the PEG-Fib-IGF group compared to the saline treatment group. These results indicate that IGF-I delivered intramuscularly via PEGylated fibrin gel, functions therapeutically in skeletal muscle recovery, from I/R mediated damage.

In a separate injury model that deals with volumetric muscle loss, IHC analyses were performed to test the efficacy of a novel tissue engineering strategy utilizing extracellular matrix (ECM) as a scaffold. In this model, also called the defect model, a 1.0 X 1.0 cm piece of the lateral gastrocnemius was removed and replaced with a muscle-derived ECM. The

constructs were then seeded with bone marrow derived cells (BMSCs), adipose derived stem cells (ADSCs) or the peroneal nerve was relocated to the area of the ECM implant. 42 days post recovery IHC analysis was performed on the ECM implants. The quantification of desmin-positive regenerating myofibers bearing centrally located nuclei, showed significantly greater values in the top, middle and bottom region of the ECM implants that received peroneal nerve relocation, when compared to the experimental group that received the ECM implant alone. Blood vessel density increases were seen within the middle region of the ECM implant groups that received BMSC+Nerve treatment and the bottom region of the ECM implant groups that received ADSC+Nerve treatment. Thus, these results corroborate the therapeutic effect of peroneal nerve relocation, which stimulated an increase in myofiber regeneration and vascular maintenance within the construct.

Table of Contents

LIST OF FIGURES

INTRODUCTION

Ischemia Reperfusion (I/R) mediated injury occurs when a tissue is reperfused following a period of ischemia and results from acute inflammation via several mechanisms. The intense nature of the inflammatory response has a local as well as a systemic response and the sequence of events leading to cell death from I/R in say a limb, can result in loss of limb function followed by multiple organ failure. Owing to this, I/R injuries have become a common clinical problem and effective therapies to remediate this injury are being developed. The ischemic phase of I/R includes the accumulation of metabolites and depletion of ATP, while the more detrimental reperfusion phase is characterized by the production of reactive oxygen species (ROS), which are oxygen-derived radicals. ROS cause severe damage to affected cell membranes and lead to cell apoptosis and/or necrosis (Blaisdell, 2002, Honda et al. 2005).

Insulin-like growth factor-I (IGF-I) is a pro-regenerative growth factor, which is upregulated locally in skeletal muscle in response to I/R mediated injury (Edwall et al. 1989, Jennische et al. 1987). IGF-I also acts as a survival factor and helps control the inflammatory response to injury (Musaro et al. 2004). IGF-I leads to a contribution of bone marrow derived cells (BMDCs) to muscle post skeletal muscle damage (Sacco et al. 2005). Importantly, post injury, in addition to stimulating satellite cell and myoblast proliferation (Barton-Davis et al. 1999, Edwall et al. 1989), IGF-I also stimulates their differentiation (Engert et al. 1996, Adi et al. 2002, Mukherjee et al. 2008). IGF-I via multiple mechanisms of action can enhance myofiber recovery. This makes it a potential therapeutic strategy for the treatment of skeletal muscle I/R mediated injury.

A synthetic material designed for tissue engineering strategies that allows for controlled release of growth factors like IGF-I is PEGylated fibrin gel matrix (PEG-Fib). In previous experiments, PEG-Fib covalently bound to a growth factor has effectively improved left ventricular function following myocardial infarction (Zhang et al. 2008, Zhang et al. 2007). Following injection and subsequent polymerization, the covalently bound growth factor is released from the PEG-Fib matrix into the local environment as degradation occurs, thereby allowing for the controlled release of growth factor from a single injection. This property makes PEG-Fib an attractive tool for growth factor therapy

following muscular injuries. Hammers et al. 2011 (unpublished) has already determined that the PEG-Fib-mediated delivery of IGF-I (PEG-Fib-IGF) improves functional recovery of skeletal muscle following I/R.

The sequence of cellular and molecular events involved in the repair of skeletal muscle is accurately regulated, especially by myogenic regulatory factors (MRFs), which are members of a family of basic helix-loop-helix proteins that act as transcription activators and regulate the transcription of muscle-specific genes (Lassar AB, 1989, Rescan PY, 2001). MyoD acts as an early MRF mainly involved in satellite cell activation and proliferation, whereas myogenin is a late-acting MRF, expressed during differentiation (Charge SB, 2004). One of the aims of this study was to localize MyoD and myogenin expression via immunohistochemistry (IHC) during the process of muscle regeneration after TK mediated I/R injury and treatment with PEG-Fib-IGF. This study uses IHC analysis to investigate the therapeutic potential of PEGylated fibrin covalently linked to IGF-I, in aiding myogenesis and/or skeletal myofiber maintenance, post I/R mediated skeletal muscle damage.

Volumetric muscle loss and subsequent functional loss are commonly seen following extremity injuries. If more than 20% of the muscle is lost, the natural repair process will fail to repair the defect. In cases of extensive traumatic injury, amputation of the injured extremity would need to be performed (Zouris et al. 2006). Surgical procedures including autologous tissue transfer may restore some function, but that does not regenerate lost muscle tissue and also risks alterations of the anatomy and biomechanics for both the recipient and the donor sites (Tu et al. 2008). As a result, a clear need exists for therapeutic strategies that can enhance the innate ability of skeletal muscle to regenerate following severe local trauma and/or induce de novo formation of functional muscle. Optimization of the therapeutic replacement of the lost tissue with a biocompatible scaffold that is capable of supporting in growth of cellular material comprises a major research area of tissue engineering. Stem cell therapy has played a significant role in the advances made in tissue engineering. Progenitor cells such as bone marrow derived mesenchymal stem cells (BMSCs) contribute to new muscle formation either through myogenic differentiation or by secretion of paracrine factors that affect the surrounding cells (Quintero et al.2009, Sun et al. 2009, Tedesco et al. 2010, Ten Broek et al.

2010). Adipose tissue derived stem cells (ADSCs) have also demonstrated the ability to differentiate towards myogenic lineages *in vitro* (Zuk et al. 2001). They are considered an attractive stem cell population for tissue engineering strategies, owing to the ease with which they can be obtained from human lipoaspirates.

Merritt et al. 2009 demonstrated that implantation of an extracellular matrix by itself is capable of supporting myofiber and blood vessel growth but does not restore function to normal levels. As a follow up study Merritt et al. 2010, implanted a 1.0 cm X 1.0 cm muscle-derived extracellular matrix (ECM) to a defect area in the lateral gastrocnemius (LGAS) of Lewis rats. Seven days later, bone marow-derived mesenchymal stem cells (BMSCs) were injected directly into the implanted ECM. 42 days post recovery, partial functional recovery occurred, with the BMSC laden ECM implant producing 85 ± 3.6% force of the contralateral LGAS. Although this was a significant improvement in the function, histological and immunohistochemical analyses of the ECM implant, showed that a hypoxic core devoid of blood vessels and cellular material was present in the ECM (middle region) that possibly restricted the complete restoration of function.

Since innervation and vascularization of the construct is critical to the outcome of muscle regeneration, the defect model was further utilized by Tierney et al. 2009 (unpublished) where stem cell therapy was supplemented with the peroneal nerve redirected to the defect area and secured to the ECM. The peroneal nerve, a neuron that innervates muscle of the anterior tibial compartment is capable of synthesizing and secreting both neural growth factor (NGF) and brain-derived neurotrophic factor (BDNF). NGF is highly expressed in regenerating skeletal muscle fibers following injury (Lavasani et al. 2006) and has been shown to stimulate the fusion of regenerating myoblasts as well as aid in the development of mature sarcomeres (Deponti et al. 2009).

Thus, for this study both BMSCs as well as adipose derived stem cells (ADSCs) were used in various combinations with the nerve relocation therapy. Functional analysis showed that all experimental groups that received the nerve relocation and Nerve+BMSC therapy saw a significant increase in specific tension compared to the matrix group. Histological analysis using trichrome showed that the middle region of ECM implants that received nerve relocation therapy had a significantly greater increase in cellular material compared to the matrix group alone.

The current investigation utilizes IHC analysis to detect the presence of regenerating myofibers and blood vessels within the defect area. The intent of this investigation was to evaluate the therapeutic ability of each cell population and the peroneal nerve relocation, in repopulating the construct.

LITERATURE REVIEW

Skeletal muscle injury

Traumatic injuries to the extremities from motor vehicle accidents or during military conflicts and increased survival following limb salvage for extremity tumors are contributing to an increasing need for better treatment options for volumetric muscle loss. In cases of significant muscle damage, infection may follow, warranting the need for amputation of the affected extremity. If surgeons decide against amputation, in favor of limb reconstruction, classic reconstruction techniques such as debridement, fracture fixation, soft-tissue management, closure and skin-grafting techniques are used (Jarvinen et al. 2006). These surgical interventions do not regenerate the lost muscle tissue although they may restore some function (Tu et al. 2008).

Common skeletal muscle injuries to skeletal muscle such as crush, contusion, laceration, ischemia reperfusion and freeze can have debilitating, prolonged effects on muscle function, even though there is no significant loss of muscle tissue (Beiner and Jokl, 2001, Garrett 1996, Jarvinen et al. 2000, 2005; Lehto and Jarvinen 1991). The current therapeutic approaches for treating muscle injuries depend on the clinical severity of injury (Jarvinen *et al.* 2005). Often, the injured muscle heals slowly and improperly regardless of treatment, leading to an incomplete functional recovery, a tendency for recurrent injuries and/or scar tissue formation (Huard *et al.* 2002).

Tissue engineering strategies work towards the efficient delivery of stem cell therapy and growth factor therapy to the areas of disease or injury. They may aim at partially or completely restoring lost muscle tissue and function. Although significant advances in the *in vitro* tissue engineering of skeletal muscle have been made in recent years (Borschel et al. 2004, Huang et al. 2005, Larkin et al. 2006, Levenberg et al. 2005, du Moon et al. 2008), the increase in knowledge of cellular and biochemical cues directing myogenesis has caused a shift in focus towards *in vivo* regenerative medicine therapies.

Skeletal muscle regeneration

Skeletal muscle has an amazing ability to regenerate post damage, relying in a large part upon the presence of mononuclear myogenic satellite cells that become activated during damage (Mauro A. 1961). The entire process of skeletal muscle repair can be divided into three phases. Soon after muscle damage, the initial destruction/inflammatory step in the skeletal muscle healing process involves the rupture of myofibers, the necrosis and phagocytosis of injured myofibers and an inflammatory cell reaction. In the repair phase, further phagocytosis of necrotic myofibers occurs, satellite cells are activated and they rapidly proliferate, fuse and differentiate to form new myofibers or repair damaged ones (Allbrook D., 1981). This phase is also characterized by the formation of scar tissue. The final remodeling phase of skeletal muscle regeneration is characterized by the reorganization of the muscle fibers, remodeling of scar tissue and restoration of muscle function.

Immediately after skeletal muscle has suffered an injury, the intracellular components of myofibers become exposed to the extracellular environment. Vascular damage also occurs within the skeletal muscle, allowing blood to leak out giving rise to a hematoma. Calcium-dependent proteases become activated and begin to rapidly destroy myofibrils. A contraction band of cytoskeletal proteins forms to protect the myofiber from complete destruction. Activation of the complement cascade allows for chemotactic recruitment of neutrophils followed by macrophages to the site of injury. The neutrophils and macrophages phagocytose necrotic fibers or release proteases that degrade cellular debris resulting from myofiber damage (Walden et al. 1990). Neutrophils and macrophages release cytokines that amplify the inflammatory response and recruit satellite cells to the injury site. Neutrophil derived superoxide has been implicated in the lysis of muscle membranes. In 2010, Tidball and Vidalta reported the existence of two disparate macrophage populations that sequentially invade injured muscle tissue. Conversely, Chazaud's group has demonstrated that at least a portion of the M1 to M2 transition is alteration in phenotypic expression rather than distinct population (Arnold et al. 2007). While the M1 macrophages are pro-inflammatory and perform the phagocytosis of necrotic fibers and promote the proliferation of satellite cells, M2 macrophages have an

anti-inflammatory effect within skeletal muscle. 24-48 hours post injury, the macrophages show an anti-inflammatory phase in which the macrophages proliferate and down regulate the inflammatory response. In fact the macrophages now aid in the transition from the inflammatory to the repair phase by releasing growth factors and cytokines. The identity of the macrophage-derived factors that influence myoblast proliferation, growth and differentiation *in vivo* remains to be determined. Candidate genes for macrophage-derived factors that may affect muscle repair include transforming growth factor-β (TGF-β) which inhibits differentiation of myogenic cells and represses expression of MyoD (Filvaroff et al. 1994). Heparin-binding EGF-like growth factor (HB-EGF) is secreted by macrophages and muscle and may increase muscle cell survival during oxidative stress (reviewed in Tidball, 2005). It has also been shown by Bondensen et al. 2004, that null mutation of cyclooxygenase-2 (COX-2) or treatment with COX-2 specific inhibitors reduced the rate of muscle regeneration and myoblast proliferation after injury. COX-2 has an anti-inflammatory effect and inhibiting it reduces the number of macrophages that infiltrate the injured area, thus impairing the muscle regenerative process.

During the repair phase, cellular material such as nerve, blood vessels and myofibers begin to infiltrate the wound area (Jarvinen et al. 2005). This phase is characterized by the activation of satellite cells, which will then migrate to the injured area, and differentiate to form myoblasts that proliferate and fuse with other myoblasts or with existing myofibers to form new skeletal muscle (Hurme, 1992, Bischoff, 1997). Quiescent satellite cells can be detected using specific markers like Pax7, cMet-R and once they become activated, they differentially express other markers like MyoD and myogenin, such that the sequence leading to addition of nuclei to existing fibers or the formation of new fibers can be tracked throughout the repair process (Charge et al. 2004).

Another group of progenitor cells capable of contributing to regeneration are a reserve compartment of resident and multipotent stem cells in the skeletal muscle called muscle-derived stem cells. These stem cells are thought to be primarily derived from the stem cells of the musculature (Peault et al. 2007). Cells from other tissues like bone marrow can also contribute nuclei to the injured area. The cells can arrive from remote locations and contribute to the formation of new muscle by undergoing myogenic

differentiation or by secreting paracrine growth factors that act on the surrounding cells (Quintero et al. 2009, Sun et al. 2009, Tedesco et al. 2010, Ten Broek et al. 2010).

The remodeling phase is an extension of the repair phase in which the newly regenerated centrally nucleated myofibers subsequently mature and form adhesions to the surrounding extracellular matrix (ECM) (Hurme et al. 1991,Kaariainen et al. 2000). The myofibers continue to mature and the expression of proteins in the reorganizing muscle, such as myosin heavy chain (MHC), transitions from developmental isoforms to mature isoforms, until the myofibers are phenotypically similar to normal myofibers (Shen et al. 2005). The regeneration process described above is not sufficient for complete recovery when there are traumatic muscle injuries of great severity, leaving areas devoid of musculature and gaps between and among remnants of the musculature that are to great to bridge. In these cases the muscle remodels leaving area devoid of muscular tissue some of which is replaced by fibrotic tissue. In this study, two types of skeletal muscle injury are studied. Damage from both types of injury namely ischemia reperfusion as well as volumetric muscle loss, is not easily reparable and the muscle shows functional impairment several days post injury. Two separate therapeutic strategies were performed for both types of skeletal muscle injury. This study seeks to evaluate via IHC, the regeneration of cellular material after administering each therapy post injury.

Skeletal Muscle Injury: Tourniquet mediated Ischemia Reperfusion(I/R)

There has been an increased interest in skeletal muscle I/R mediated injury due to the significant extremity injuries sustained by soldiers during recent wars undertaken by the US. In military conflicts, extremity injuries sustained due to high energy blasts result in extensive bone and soft tissue damage. To treat these injuries, tourniquets may be applied during evacuation. After removal of the tourniquet, I/R leads to additional injury owing to acute inflammation via several mechanisms. Skeletal muscle, which is the primary tissue in a limb for example, is most vulnerable to I/R-mediated damage. This inflammatory response is required to dispose of necrotic tissue and initiate the healing process.

Local and systemic damage due to I/R can be attributed to reactive oxygen species (ROS) and activated neutrophils. ROS are activated oxygen derived radicals like the

superoxide anion (O_2^-), hydrogen peroxide (H_2O_2), hydroxyl radical (OH), hypochlorous acid (HOCl) and nitric oxide-derived peroxynitrite (Reviewed in Gillani et al. 2011). These radicals are produced in a reaction involving the enzyme xanthine oxidase (XO), which is derived from an oxidized nicotinamide-adenine dinucleotide (NAD+)-dependent dehydrogenase (XDH) in ischemic conditions. ATP depletion occurs during ischemia because ATP is broken down to hypoxanthine. Upon reperfusion, oxygen is made available which is utilized in the XO-catalysed ROS formation (Granger et al. 1988, Moriwaki et al. 1999, Smith et al. 1989).

ROS are oxidizing and reducing agents that can cause cell membrane damage via lipid peroxidation, and in turn by neutrophil activation (Tokoyuni S, 1999). Cell membrane damage activates cyclooxygenase and lipoxygenase pathways as well as transitional metal ions, which further cause damage via lipid peroxidation in neighboring tissues. Products of the lipoxeganse pathway stimulate neutrophil activation. Neutrophils contain four types of intracellular granules, which release their products upon activation.

Azurophilic granules contain myeloperoxidase (MPO), which besides producing oxidants also catalyses the reaction of hydrogen peroxide with chloride ion to form hypochlorous acid (HOCl). HOCl then reacts with other molecules to form reactive oxygen species with high potential for tissue damage. Specific granules and their products may have a role in complement system activation (Wright DG, 1977). They also contain collagenase and apolactoferrin, which enable neutrophils to adhere to the site of inflammation (Oseas, 1981). Gelatinase or tertiary granules are involved in functional utility of the surface protein. The leakage of the neutrophils causes cell damage and is also associated with inflammation (Kjeldsen, 1994).

Secretory granules may also play functional roles as surface proteins. During reperfusion, the activated leucocytes will adhere to the endothelial layer and will ultimately result in endothelial disruption (Weiss SJ, 1989). Additionally, activated leucocytes can transmigrate through the post capillary venules to the interstitial space and induce microvascular barrier disruption by releasing ROS and cytotoxic enzymes. This allows plasma proteins to leak into the interstitial space and increase the interstitial fluid pressure. This compresses the capillaries leading to the no-reflow phenomenon, the

outcome of which is that the metabolic demands of the muscle are not met during reperfusion leading to muscle necrosis.

During ischemia, skeletal muscle tissue is faced with a cascade of ATP depletion, acidosis, and ion imbalance. The reentry of blood flow to the area, reperfusion, is much more damaging, as it causes production of reactive oxygen species (ROS) and rapid calcium influx into the cell; both of which cause mitochondrial dysfunction that will ultimately lead to cellular apoptosis and/or necrosis (Honda 2005).

Previous studies (Hammers et al. 2008 and Walters et al. 2008) have demonstrated histological pathology and large functional deficits in the skeletal muscle of rodents following TK-induced I/R. Walters et al. 2008 demonstrated that at 14 days following 4 hours of IR injury, complete recovery of muscle function is not achieved. Fish et al. 1993 showed that 42 days post a 2 hour ischemia, muscle recovery had not taken place, as maximal force production in the ischemic reperfused muscles was still lower than the contralateral uninjured muscles. Several tissue-engineering strategies are in the pipeline to serve as potential therapies for regeneration of skeletal muscle post I/R mediated damage.

Insulin-like Growth factor-1 and its role in skeletal muscle repair

Insulin-like growth factor-I (IGF-I) is a circulating endocrine growth factor, which is released in autocrine/paracrine fashion from skeletal muscle in response to injury and mechanical stimuli. IGF-I stimulates both proliferation and differentiation in satellite cells (Engert et al. 1996, Florini et al. 1999). Skeletal muscle injury increases IGF synthesis by satellite cells in rodents, stimulating satellite cell proliferation and differentiation into myoblasts (Barton-Davis, E.R. et al. 1999, Edwall D et al. 1989). IGF-I is unique in that it stimulates both myoblast proliferation and differentiation (Engert et al. 1996; Chakravarthy, MV et al. 2000, Mukherjee et al. 2008). Although it seems that IGF-I has two contradictory roles, the co-operation of IGF-I with other mitogenic or myogenic differentiation signals stimulates either or both of the aforementioned events.

In proliferating myoblasts, IGF-I increases the expression of cell-cycle progression factors and is needed for cells to traverse the G1 phase of the cell cycle (Engert et al. 1996, Lowe WL, 1991). After withdrawal of myoblasts from the cell cycle IGF-I promotes muscle differentiation by inducing the expression or activity of myogenic regulatory factors (Musaro and Rosenthal, 1999). It has been seen under most *in vitro* conditions that high IGF-I concentrations favor proliferation, whereas lower IGF-I concentrations seem to promote differentiation (Coolican, SA et al. 1997). IGF-I activates several signaling pathways in skeletal muscle. Previous studies (Coolican et al. 1997, Jones et al. 2001, Tamir & Bengal, 2000) have suggested that the mitogen-activated protein kinase (MAPK) mediates cellular proliferation, whereas the phosphatidylinositol 3-kinase (PI3K) pathway is activated during differentiation.

The PI3K/Akt signaling pathway is the predominant pathway that stimulates muscle protein synthesis and is believed to be required for a normal hypertrophic response, via activation of mTOR and inhibition of FOXOs (Bodine et al. 2001, Latres et al. 2005, Rommel et al. 2001, Sacheck et al. 2004, Stitt et al. 2004). Under normal conditions, Akt activation signals the formation of TORC1, a complex of which mTOR is an important component (Pallafachina et al. 2001). Activation of mTOR signals the phosphorylation of p70S6K and 4EBP1. While p70S6K phosphorylates a ribosomal subunit that is responsible for muscle protein translation, the translation repression activity of 4EBP1 is inhibited following its phosphorylation (Ohanna et al. 2005, Hara et al. 1997). IGF-I is also capable of altering transcription and translation of muscle factors that regulate myocyte growth or differentiation (Jacquemin V et al., 2007, James PL et al., 1996). For example, IGF-I inhibits production of myogenin, a muscle differentiation protein, thereby promoting proliferation of myoblasts. However, prolonged exposure of IGF-I will result in increased myogenin expression, thus promoting differentiation (Tureckova J et al., 2001). IGF-I also modulates differentiation by controlling the expression of MyoD, myocyte enchancer factor-2 and p21. IGF-I inhibits the expression of atrogin-1 and muscle ring finger-1 protein (MuRF-1), proteins that target muscle proteins to protosomes for degradation (Sachek, J.M. et al, 2004).

IGF-I is locally upregulated in skeletal muscle in several injury models including cardiotoxin injury (Hill et al. 2003 and 2003, Jennische et al. 1987). Owing to the

mitogenic, myogenic, hypertrophic and antiapoptotic/prosurvival actions of IGF-I on skeletal muscle (Kooijman et al. 2006, review), it was selected to provide growth factor therapy, via intramuscular mode of delivery for skeletal muscle that had undergone I/R mediated damage (Hammers et al. 2011, unpublished).

The role of PEGylated fibrin gel as a therapeutic delivery vehicle

Polyethylene glycol modified (PEGylated) fibrin is a novel biomaterial developed by Suggs et al. 2007, that can covalently bind growth factors and allow for their prolonged release. Fibrin is the primary protein component of this biomaterial and has been used as a Food and Drug Administration-approved surgical adhesive and sealant. The Pharmaceutical industry widely uses the technique of protein PEGylation, which is the covalent coupling of soluble PEG to proteins. The benzotriazole carbonate derivative of polyethylene glycol (SG-PEG-SG) can be used to PEGylate fibrinogen. PEGylated fibrin gels are injectable with the formation of the biomatrix catalyzed by the addition of thrombin to PEGylated fibrinogen. After combining both components, the solution remains in liquid form for about 1-2 minutes before polymerization. It can therefore be mixed *in vitro* and injected by syringe into the tissue of concern via a specially designed catheter to achieve a minimally invasive procedure. To use PEGylated fibrin as a delivery vehicle for growth factors, the appropriate growth factor can be bound to the PEGylated fibrinogen via the electrophilic groups at the ends of the SG-PEG-SG. In previous experiments, a polyethylene glycol (PEG)-ylated fibrin gel (PEG-Fib) matrix containing covalently bound growth factor has effectively improved left ventricular function following myocardial infarction (Zhang G et. al 2007, Zhang G et. al, 2008). Following injection and subsequent polymerization, the covalently bound growth factor is released from the PEG-Fib matrix into the local environment as degradation occurs, thereby allowing for the controlled release of growth factor from a single injection. This property makes PEG-Fib an attractive tool for growth factor therapy following skeletal muscle injury.

In the repair of skeletal muscle damage incurred by I/R injury, the combination of IGF-I delivered via PEG-ylated fibrin gel matrix could prove to be a powerful therapeutic

strategy. Hammers et al. 2011 (unpublished) has demonstrated the release kinetics of IGF-I from PEG-Fib *in vitro*, using ELISA. The data shows that the majority of IGF-I is released from the matrix within the first 24 hours; however a physiologically relevant dose of ~ 12 ng/ml was measured at 96 hours. Analysis of IGF-I release by Western blotting showed that immunoreactive IGF-I is released as IGF-I peptides rather than large complexes. The same study also showed substantial functional improvement in the PEG-Fib-IGF treatment group compared to saline and PEG-Fib treatment groups (Fig. 1). These results indicate that the PEG-Fib-IGF treatment has therapeutic potential for skeletal muscle I/R. The current study will evaluate the efficacy of the PEG-Fib-IGF therapy, using immunohistochemical techniques.

Skeletal muscle injury: Volumetric muscle loss defect model and the therapies being evaluated in this study.

Skeletal muscle tissue can be decellularized and made devoid of all cellular material. All that remains following the decellularization procedure is an extracellular matrix (ECM) primarily composed of collagen and void of all cellular material and soluble proteins, rendering it nonimmunogenic. The protocol was first developed by Borschel et al. 2004 and modified and applied by Merritt et al. 2009. The three dimensional geometry of the decellularized ECM allows for the transduction of mechanical force throughout the construct. The decellularized ECM has been shown to be capable of supporting and guiding myofiber ingrowth (Borschel et al. 2004, Merritt et al. 2009) and retains the specific and complex infrastructure necessary for recellularization of vascular bed and peripheral nervous system (Kochupura et al. 2005). Conconi et al. 2005 demonstrated the benefits of using decellularized abdominal muscle, seeded with myoblasts as a tissue engineering strategy for skeletal muscle. The group found that when implanted in the abdominal wall, the constructs generated a complex skeletal muscle tissue that was contractile and vascularized after only 9 days. Borschel et al. 2004 was able to produce skeletal muscle capable of contraction by seeding myoblasts on a decellularized ECM *in vitro.*

The defect model created in the lateral gastrocnemius (LGAS) of rats comprised of the creation of a 1 cm X 1 cm defect, which was replaced by a skeletal muscle derived ECM, also 1 cm X 1 cm in dimension. In a previous study by Merritt et al. 2009 it was shown that the ECM implantation by itself does not restore function. Later, Merritt et al. 2010 also evaluated the therapeutic effect of injecting bone marrow derived mesenchymal stem cells (BMSCs) into an implanted ECM. *In situ* functional measurement of the rats that received therapy showed that the maximal isometric tetanic force produced by the LGAS of the ECM-BMSC group was significantly higher after 14, 28 and 42 days of recovery than the force of ECM-ONLY. When the defect implant was examined histologically by region (top, middle and bottom), the appearance of cellular material and blood vessels was less evident in the ECM-ONLY group compared to the ECM-BMSC group. However, the middle region for the ECM-BMSC group showed significantly fewer myofibers than the respective top and bottom regions that bordered the transected myofibers. Thus, the injection of BMSCs by itself was not successful in promoting regeneration of cellular material at the center of the ECM implant.

A study by Tierney et al. 2009 (unpublished) sought to overcome the problem of the hypoxic core by incorporating additional therapies to the defect model, namely adipose derived stem cell (ADSC) therapy and relocation of the peroneal nerve to the implanted ECM. A significant increase in specific tension was seen in all groups that underwent the nerve relocation procedure, rising 11.0%, 14.3% and 11.5% in the Nerve, the BMSC+Nerve and the ADSC+Nerve groups (Fig. 2) respectively, when compared to the ECM-only group. The current study seeks to evaluate the therapeutic potential of the various combinations of the aforementioned treatments by utilizing immunohistochemical markers for skeletal muscle fibers, namely the muscle specific protein Desmin as well as to evaluate vascularization within the construct by identifying blood vessels utilizing PECAM-1, a marker for endothelial cells.

<u>The role of bone marrow derived mesenchymal stem cells in skeletal muscle repair</u>

The improved functional and histological regeneration observed after 42 days in the ECM-BMSC group described in Merritt et al. 2010 as well as Tierney et al. (2009 thesis-unpublished) is likely the result of a number of different positive effects attributed to the

implanted BMSCs. MSCs are multipotent cells that can give rise to osteocytes, adipocytes and chondrocytes *in vitro* (Pittenger et al. 1999, Zuk et al. 2002, Baksh et al. 2004). LaBarge and Blau, 2002 proved that endogenous cells from the bone marrow participate in muscle regeneration due to physiologic stress. While the participation of these bone marrow cells in muscle regeneration appears to be rare (<3.5%), they progress from the bone marrow and into the muscle where they become progenitor cells and/or satellite cells that can be activated in response to muscle injury (LaBlarge and Blau, 2002). In studies utilizing the Mdx mouse model of Duchenne muscular dystrophy, bone-marrow-derived progenitor cells became incorporated into skeletal muscle and were found to occupy the satellite cell niche (Bittner et al. 1999, Fukada et al. 2002, Saito et al. 1995, Quintero et al. 2009). Literature also shows that BMSCs are capable of myogenic differentiation *in vitro* when induced under suitable conditions (Wakitani et al. 1995, Dezawa et al. 2005). An additional benefit of using bone marrow derived stem cells and adipose derived MSCs is that, in cases of significant muscle loss (such as the defect model of volumetric muscle loss), these multipotent stem cells can contribute to the restoration of other vital components of skeletal muscle such as nerves and blood vessels which are also lost owing to the injury (Ladak et al. 2011, Guidicci et al. 2010, Tille and Pepper 2002).

Merritt et al. 2010 as well as Tierney et al. 2009 (unpublished) were able to demonstrate that injection of BMSCs into the implanted ECM results in an improved functional output. Differentiation into myofibers or fusion with existing myofibers may play a role in these improvements. BMSCs have been shown to participate in autocrine/paracrine signaling mechanisms that stimulate or directly cause the release of growth factors, cytokines and chemokines (Prockop, 2009). In the defect study, post BMSC therapy, increases in cellular content occurred primarily in the top and bottom regions adjacent to transected myofibers, suggested that the ingrowth of injured myofibers occurred from the superior and inferior portions of the muscle remaining after the defect injury. Thus, in the defect model of volumetric muscle loss, BMSC therapy was not potent enough to allow myofibers and blood vessels to transect through the middle portion of the ECM implant.

The role of adipose derived stem cells in skeletal muscle repair

The ease and efficiency of surgical isolation as well as increased potential for point-of-care preparation of the cell concentrate make adipose derived stem cells (ADSCs) an attractive alternative to BMSCs. ADSCs demonstrate the same multipotency and myogenic differentiation capacity as other mesenchymal progenitor cells (Pettersson et al. 1984, Zuk et al. 2001, Gimble and Guilak 2003). ADSCs could also prove useful as a source of injectable progenitor cells, since they are present at a high density, allowing the possibility of direct injection without the need for prolonged culture *in vitro* (Padoin et al. 2008).

However, the study by Tierney et al. 2009 (unpublished) determined that ADSCs were unable to improve functional recovery of a skeletal muscle defect repaired with an implanted ECM. ADSCs can be induced to differentiate towards a myogenic lineage *in vitro* (Mizuno et al. 2002). However, expression of markers characteristic of another cell type does not necessarily result in a functioning cell type under normal physiological conditions *in vivo.* Removal from their stromal microenvironment may induce differentiation and alter phenotypic expression patterns, while their implantation may alter those expression patterns induced *in vitro*.

Reinnervation and vascularization of a skeletal muscle construct

The reinnervation of the regenerating myofibers plays a critical role in determining the regeneration potential of injured muscle. An important step in any regenerative medicine strategy for volumetric muscle loss is to ensure the reestablishment of nerves to the regenerating muscle and the formation of new motor endplates. If neuromuscular connections are not established then the regenerated muscle will atrophy and die (Jarvinen et al. 2005, 2007). Dhawan et al. 2007 demonstrated that *in vivo* innervation of a muscle construct results in increased contractility compared with non-innervated constructs. The relocation of the peroneal nerve (Jansen et al. 1973) may be able to benefit the regenerative process via neurotization and the formation of new ectopic motor endplates, resulting in the sustained survival and function of regenerating myofibers (Payne & Brushart 1997). Direct contact of the relocated peroneal nerve with a viable motor

endplate can lead to successful reinnervation of a denervated or regenerating myofiber (Bixby & Van Essen 1979).

Hence, Tierney et al. 2009 (unpublished) redirected the peroneal nerve in rats to the ECM implanted in the lateral gastrocnemius muscle. The peroneal nerve was denervated as distally as possible and redirected through the anterior and posterior compartments to secure it to the lateral surface of the ECM implant. Oriented within the defect area and perpendicular to myofibers of the LGAS, the nerve was secured to the ECM with a suture. The groups that did receive the nerve relocation saw a significant increase in specific tension when contractile activity in the muscle was recorded, rising 11%, 14.3% and 11.5% in the Nerve, Nerve+BMSC, Nerve+ADSC groups when compared to the ECM only group. Upon performing histological analysis it was seen that all groups that did receive the nerve relocation saw a significant increase in cellular content of the middle region when compared to all groups lacking this treatment.

Thus this current study will further evaluate using immunohistochemistry, the efficiency of the bone-marrow derived stem cell therapy, adipose-derived stem cell therapy and nerve relocation procedure applied in various combinations towards the treatment of the defect using a skeletal muscle derived extracellular matrix (ECM) as a scaffold. A muscle specific antibody against Desmin will be used to identify regenerating myofibers within the ECM. This study also seeks to evaluate the maintenance of blood vessels within the ECM area post the different therapies using the endothelial cell marker, PECAM-1.

SIGNIFICANCE OF STUDY

This thesis undertakes the immunohistochemical evaluation of skeletal muscle health and regeneration in two distinct models of skeletal muscle injury. The first injury model discussed is ischemia reperfusion mediated injury and the second is a volumetric muscle loss model, also known as the defect model of muscle injury. Both types of injury are commonly seen during military combat and also during civilian-related accidents, and result in sustained functional deficits depending on the severity of the damage incurred.

While the American soldiers fearlessly undertake their responsibilities on the battlefield, vowing to protect their country, researchers in the field of tissue engineering strive to develop novel effective therapies for the wounds inflicted upon the soldiers during combat. Proper rehabilitation in conjunction with an effective treatment to reverse both tissue loss and function loss, would allow these soldiers, both men and women to function as active and independent members of society.

The work done in this study is a follow up assessment of two different therapeutic strategies utilized for each of the two injuries, but performed within the same laboratory. For the I/R study, the results presented here will contribute to the field of tissue engineering, by determining whether synthetic Polyethylene glycol (PEG)-fibrin biomatrix can be used effectively to deliver growth factors via local intramuscular injection into skeletal muscle. The ease of administering this therapy post damage could potentially make it popular among clinicians.

For the defect study, the results presented here will make shed light on the therapeutic potential of bone-marrow derived stem cells, adipose-derived stem cells and peroneal nerve relocation procedure in skeletal muscle regeneration. The results will pave the way for further research to promote the reinnervation and revascularization of regenerated skeletal muscle.

METHODS

Ischemia reperfusion study:

All tissue samples for this study were obtained from Sprague Dawley rats (Charles River Laboratories, Wilmington, MA) 6-9 months of age. The rats were housed individually, maintained on a 12-hour light/dark cycle and allowed *ad libitum* access to food and water. The rats were randomly assigned to experimental groups and were evaluated functionally first (Hammers et al. 2011, unpublished) and histologically, after 14 days of recovery. Immunohistochemistry was performed on tissue samples from 3 different rats per experimental group. All animals were obtained from the Animal Resource Center at the University of Texas at Austin and treated in compliance with the ethical guidelines of the Institutional Animal Care and Use Committee (IACUC).

Defect study:

All tissue samples for this study were obtained from Lewis rats (Charles River Laboratories; Wilmington, MA) 6-9 months of age. The rats were housed individually, maintained on a 12-hour light/dark cycle and allowed *ad libitum* access to food and water. Rats were randomly assigned to experimental groups and were evaluated functionally first (Tierney et al. 2009) and then histologically following 42 days recovery. Immunohistochemistry was performed on tissue samples for 3 different rats per experimental group.

An overview of the protocol employed by Hammers et al. for the ischemia reperfusion study.

A 2-hour Tourniquet (TK) induced I/R was performed on the rats. A single, randomly selected hindlimb was elevated, and a pneumatic TK (Hokanson) was wrapped snugly against the proximal portion of the limb and inflated to 250 mmHg by the Portable Tourniquet System (Delfi Medical Innovations) to ensure complete occlusion of blood flow to the limb for 2 hours. Body temperature was maintained with the use of a heat lamp during this procedure. After 2 hours, the pneumatic TK was removed, and the rat was returned to its cage for recovery. During the course of this procedure, the rats were anesthetized with 2% isoflurane.

Bifunctional SG-PEG-SG (NOF America Corp) was reacted with reconstituted porcine fibrinogen (Sigma; molar ratio of 5:1 for PEG: Fibrinogen) and hIGF-I (Peprotech). Polymerization was induced by the addition of 25 U/mL human thrombin (Sigma). The final concentration of IGF-I was 25μg/mL.

Twenty-four hours following release of the TK, 0.25mL of either sterile PBS (saline;n=8), bolus IGF-I (bIGF; 25 μg/mL;n=4), empty PEGylated fibrin gel (PEG-Fib; n=6), or IGF-I conjugated PEGylated fibrin gel (PEG-Fib-IGF; n=6) was injected into the lateral gastrocnemius (LGAS) of the TK-injured limb. All injections containing PEG-Fib occurred before matrix polymerization. Animals were allowed 14 days of reperfusion prior to functional assessment.

In a subsequent experiment, 0.25mL of PEG-Fib (n=4) or PEG-Fib-IGF (n=4) was injected in the same manner, while animals were allowed 4 days of reperfusion. LGAS muscles were harvested from euthanized animals, frozen in liquid nitrogen-cooled isopentane, and stored at -80°C until further analysis.

After 14 days of reperfusion, functional assessment of LGAS force production was performed in situ. After the completion of contractile measurements, the muscles were dissected free, weighed, imbedded in OCT compound, frozen in liquid nitrogen-cooled isopentane, and stored at -80°C until further analysis. LGAS measurements of non-injured limbs were used for non-TK control values (n=14).

An overview of the protocol employed by Tierney et al. for the defect injury study

The extracellular matrix (ECM) used as a scaffold in all the experimental groups for this study was prepared by using a decellularization protocol described in Tierney et al. 2009 (thesis). ECMs were derived from gastrocnemius muscles of Lewis rats by conducting several washes in deionized water, chloroform, 2% SDS (a potent detergent to wash off cellular material) and several rinses with deionized water.

Bone marrow was obtained from the surgically removed femur and tibia of Lewis rats by flushing the shaft with media using a 10mL 18G syringe. Cells were disaggregated by gently pipetting and centrifuged at 1000g for 5 min at 4°C. The resulting pellet was resuspended in media, plated on conventional tissue culture plates in a non-inductive control medium containing Dulbecco's modified eagles medium (DMEM), 10% fetal bovine serum (FBS) and 1% antibiotic/antimycotic (AA) solution and incubated overnight at 37°C and 5% CO_2. The resultant adherent fraction was rinsed and maintained at 37°C and 5% CO_2 and passaged as the cells reached 70% confluency.

Adipose derived stem cells were obtained from rat lipoaspirates following a protocol described by Zuk et al. 2001. To isolate the stromal vascular fraction (SVF), raw lipoaspirate was washed extensively with equal volumes of phosphate buffered saline (PBS). Washed aspirates were treated with 0.075% collagenase in PBS for 30 minutes at 37°C. Enzyme activity was neutralized with Dulbecco's modified Eagle's medium (DMEM) containing 10% fetal bovine serum (FBS) and 1% AA solution. High-density SVF pellets were obtained by centrifugation at 1200g for 10 min and resuspended in 160 mM ammonium chloride for 10 minutes at room temperature to lyse contaminating red blood cells.

Centrifugation was repeated (1200g for 10 min) and SVF pellets were filtered through 100-μm nylon mesh to remove cellular debris. The filtrate was plated on conventional tissue culture plates in a non-inductive control medium as that used for BMSCs, and incubated overnight at 37°C and 5% CO_2. Plates were washed extensively with PBS to remove residual non-adherent cells. The resultant adherent fraction was maintained at 37°C and 5% CO_2 and passaged as the cells reached 70% confluency.

Before surgical procedures, animals were randomly placed in one of six experimental groups: implantation of the ECM (MAT), implantation of the ECM followed by ADSC injection (AD), implantation of the ECM followed by BMSC injection (BM), implantation of the ECM followed by redirection of the peroneal nerve (N), implantation of the ECM followed by peroneal nerve redirection and BMSC injection (BM+N) and implantation of the ECM followed by redirection of the peroneal nerve and ADSC injection (AD+N). All surgeries were performed under aseptic conditions and with sodium pentobarbital (65mg/kg body weight) anesthesia via intraperitoneal injection.

All animals underwent the defect surgery wherein a 1 cm X 1 cm defect was created in the lateral gastrocnemius muscle. An ECM of the same dimension was then attached to the defect area by using a modified Kessler stitch. MSC injections were performed following a 7 day recovery period, where the lateral gastrocnemius was re-exposed and approximately 1.5 million MSCs suspended in PBS were injected at several points in the ECM. Groups classified under peroneal nerve relocation, underwent surgery where the peroneal nerve was denervated as distally as possible and redirected through the anterior and posterior compartments to the defect area. The end of the nerve was secured to the ECM.

Following the recovery period, *in situ* measurements were performed on both the experimental leg and the contralateral, undamaged leg. Total force and specific tension produced by the LGAS were measured.

Immunohistochemical analysis

After functional analysis was performed, the experimental LGAS was excised, cleaned off excess fat and external connective tissue, weighed and placed on a piece of soft wood coated with a mixture of Tragacanth gum and OCT. The piece of wood with the attached piece of tissue was then immersed in isobutane at -150 degrees Celsius cooled in liquid nitrogen. The frozen tissue was then stored in aluminum foil at -80 degrees Celsius, or sectioned immediately for analysis.

Series of 5 μm cross sections were taken from within the central regions of the LGAS muscle and were made using a Leica CM1900 cryostat microtome (Leica Microsystems; Wetzlar, Germany) at -20 degrees Celsius. The sections were allowed to dry overnight at room temperature.

In preparation for immunofluorescent identification, sections were fixed in acetone for 8-10 minutes. After which, they were washed in phosphate buffered saline (1X, PBS) and blocked with 5% normal donkey serum in PBS containing 1% bovine serum albumin (BSA). All of the following materials were purchased from Santa Cruz Biotechnologies, Santa Cruz, CA.

For the I/R study, sections were first incubated with primary antibodies against cytoskeletal protein desmin (1:200, goat polyclonal), immature myofiber marker neonatal myosin (1:200, mouse monoclonal), myogenic regulatory factors MyoD and Myogenin (1:200, rabbit polyclonal).

For the Defect study, sections were first incubated with primary antibodies against desmin (1:200, goat polyclonal) and endothelial cell marker PECAM-1 (1:50, goat polyclonal).

All sections were detected with donkey anti-goat IgG-FITC fluorescein (1:100, λ=495 nm), donkey anti-rabbit-FITC fluorescein (1:100, λ= 495 nm) or a donkey anti-mouse IgG-TRITC fluorescein (1:100, λ=546 nm), depending on the primary antibody used.

Finally, all sections were counterstained with DAPI (1:1000, λ=425 nm) to identify nuclei. Following a final series of washes in PBS, sections were mounted in Permount mounting medium (Fisher Scientific; Waltham, MA).

Imaging and analysis:

Immunofluorescence was visualized with a Leica DM LB2 fluorescence microscope and photographed with a Leica DFC340FX digital camera (Leica Microsystems; Wetzlar, Germany).

Defect study: At each level and within each region of the ECM, the number of intact myofibers expressing desmin was counted using Image J and expressed as a percentage of the total number of myofibers in the ECM area. Also, the number of PECAM-1 positive blood

vessels were counted in each image and expressed as the number of blood vessels present per unit area of the ECM (#/mm^2). A vessel was only counted if its lumen was greater than 20 μm in diameter.

Ischemic Reperfusion study: For immunohistochemical quantification, the total number of nuclei co-expressing DAPI and MyoD or Myogenin were counted using Image J and expressed as a percentage of total nuclei present in the image area. Desmin was used as a potential indicator of cell viability and the number of intact myofibers expressing desmin was counted using Image J and expressed as a percentage of the total number of myofibers in the image area. Neonatal myosin was used to detect the newly formed muscle fibers which were expressed as a percentage of the total number of myofibers in the field of the image.

Statistical Analysis

For the I/R study, all values are represented as mean ± SEM. Statistical analysis was performed using a one-way ANOVA (Tukey's post hoc test, α=0.05). Student t-tests were performed to determine significance between means.

For the defect study, all values are represented as mean ± SEM. Statistical analysis was performed utilizing three-way ANOVA for analysis of group samples. Comparisons between data sets were performed utilizing a priori student's t-tests and Tukey's post hoc tests where available. Statistical significance is defined as $p<0.05$.

RESULTS

Ischemia Reperfusion Study

Immunohistochemical analysis

MyoD colocalization with DAPI was assessed in the tissues that were harvested at 4 and 14 days post recovery. At 4 days, the PEG-Fib group showed a negligible expression of MyoD and DAPI at 0.434±0.25%. In the same group the co-expression of DAPI and MyoD increased to 8.8±1.5% at 14 days. At 4 days of recovery, the PEG-Fib-IGF group showed negligible co-expression of MyoD and DAPI at 0.17±0.03%. There was an increase in this value seen in the 14 day animals with 2.4±0.9% of the total nuclei in the field of the image expressing both MyoD and DAPI (Fig. 3). At 14 days, compared with the PEG-Fib and PEG-Fib-IGF-I groups, the saline group showed a significantly higher ($p=0.007$ and $p= 0.002$ respectively) percentage of nuclei co-expressing DAPI and MyoD at 33.7±4.4 (Fig. 4A,B).

Myogenin co-localization with DAPI was also assessed in the tissues. At 4 days, the PEG-Fib group showed the nuclear expression of Myogenin to be at 2.0±0.9% and an increase in expression was seen at 14 days to be at 18.3±9.4%. At 4 days of recovery, the PEG-Fib-IGF-I group showed the nuclear expression of myogenin to be at 3.6±1.74% of the total nuclei present per field of the image. At 14 days, this value decreased to 1.9±0.9% (Fig. 3). The saline group, post 14 days of recovery showed a significantly higher percent nuclear co-localization of myogenin and DAPI at 44.1±7.4% than the PEG-Fib-IGF group ($p=0.009$) (Fig. 5A,B).

Desmin was used as an indicator of muscle cell viability and differentiation. Myofibers that were damaged showed very low or no desmin expression at all. The fibers that were positive for desmin expression were counted and expressed as a percentage of the total number of myofibers in the field of the image. At 4 days, the PEG-Fib and PEG-Fib-IGF groups showed 45.8±8.3% and 51.6±9% healthy fibers respectively. At 14 days, the

percentages of desmin positive healthy myofibers for these two groups were 44.6±1.5% for PEG-Fib and 88.8±3.7% for PEG-Fib-IGF-I (Fig. 3). Thus for the later group, there was a significant increase in the percentage of desmin positive fibers at 14 days compared to 4 days ($p=0.04$). Desmin expression in the saline group at 14 days remained significantly lower ($p<0.001$) than the PEG-Fib-IGF-I group (Fig. 6A,B).

Neonatal Myosin expression in the myofibers was evaluated as an indicator of cell immaturity, as it is rarely present in adult muscle. At 4 days, the total percent of myofibers expressing neonatal myosin in the PEG-Fib group was seen to be at 18.8±4.7%. This expression increased to 32.9±9.5% at 14 days. The trend in the PEG-Fib-IGF-I group was the opposite with a greater expression of 27.6±3.1% seen at 4 days than the low value of neonatal myosin expression 7.7±2.7% observed at 14 days (Fig. 3). In the saline group the percentage of myofibers that expressed neonatal myosin per field of image was 35.1±5.5%. Thus at 14 days, the neonantal myosin expression in the PEG-Fib-IGF-I group was significantly lower than both the saline ($p=0.004$) and PEG-Fib ($p=0.034$) groups (Fig. 7A,B).

Defect Model Study

Immunohistochemical Analysis

Desmin is an early structural cytoskeletal protein arranged in sarcomeric form within a myofiber. Desmin was used as a marker to detect and quantify the regenerated myofibers found within the area of the ECM. All fibers that were counted showed the presence of a centrally located nucleus as detected by the DAPI counter stain. Regenerating myofibers contained within the ECM following peroneal nerve relocation occupied a significantly greater area than the Matrix group. This significance was seen in all three regions of the ECM, namely the top, the middle and the bottom regions ($p=0.03$, $p=0.02$ and $p=0.02$ for each of the three regions respectively). BMSC or ADSC therapy alone did not make a significant contribution to cellular content in any of the three regions when compared to the Matrix group. However, when the cellular therapy was supplemented

with the peroneal nerve relocation, the bottom region of the BMSC+nerve group showed a significant increase in cellular material compared to the bottom region in the Matrix group ($p=0.04$). The middle and bottom regions of the ADSC+Nerve group showed an increase in cellular material ($p=0.02$ for mid. and $p=0.009$ for bot.) compared to the Matrix group. Thus at least one region in all three experimental groups that received peroneal nerve relocation therapy showed a significantly greater amount of cellular material than the corresponding region in the Matrix only group (Fig. 8,9).

PECAM-1 (CD31) was used to determine the density of blood vessels (per mm^2) within the ECM. It is a marker for endothelial cells as it makes up a large part of the endothelial cell intracellular junctions. The middle region of the BMSC+Nerve group showed a significantly greater blood vessel density than the middle region of the Matrix group ($p=0.04$). Also the bottom region of the ADSC+nerve group showed a significantly greater blood vessel density than the bottom region of the matrix group ($p=0.002$). This group showed a significantly greater maintenance of blood vessels compared to the bottom region of the ADSC injection group ($p=0.007$) (Fig. 10,11).

DISCUSSION

Ischemia Reperfusion Study

Injection of PEGylated fibrin gel covalently linked to IGF-I, into the gastrocnemius of rats following tourniquet mediated ischemia reperfusion showed a recovery of function to levels that were not significantly different from the control undamaged muscle (Hammers et al. 2011, unpublished) (Fig. 1). Genetic over-expression of IGF-I has been shown to facilitate muscle regeneration following traumatic injury (Pelosi et al. 2007), thus making it a molecule of choice for therapy following muscle injury. Immunohistochemical (IHC) analysis of the tissues harvested at 4 days and 14 days post damage sheds light on the effective therapeutic application of IGF-I delivered via the PEGylated fibrin biomatrix.

MyoD and myogenin are myogenic regulatory factors (MRFs) that play an important role in the activation and differentiation of muscle satellite cells (Rantanen et al. 1995). MyoD functions in determining the myogenic fate of satellite cells, whereas myogenin appears to function in the activation of terminal muscle cell differentiation (Montarras et al. 1991, Andres et al. 1996). The mRNA and protein for MyoD was detected in activated satellite cells a few hours after injury (Grounds et al. 1992, Fuchtbauer and Westphal, 1992), hence MyoD has been in use as an immunohistochemical marker for activated satellite cells.

The quantification of IHC data shows that the skeletal muscle fibers in the saline group at 14 days show a higher MyoD and myogenin colocalization with their nuclei, compared to the PEG-Fib-IGF-I group. The high levels of expression of MyoD and myogenin suggest that the satellite cells located at the surface of the degenerating or regenerating myofibers may still be activated and required to participate in the processes of delayed myogenesis, in the saline injection group. Thus these results indicate that intramuscular therapy of PEGylated IGF-I perhaps intensifies muscle regeneration or prevents muscle degeneration, after I/R.

It has been seen in previous studies that the level of MyoD and myogenin mRNA increases in the skeletal muscle of aged animals (Musaro et al. 1995, Marsh et al. 1997, Gomes and Booth 1998, Lowe et al.1998, Kostrominova et al. 2000, Alway et al. 2001) Western Blots to detect protein expression of the two myogenic regulatory factors in aged

muscle, showed that both MyoD and myogenin protein levels were higher in aged rats compared to young rats. The pattern of MyoD protein expression in aged gastrocnemius muscles is reminiscent of that detected in denervated muscles of 4-month-old rats (Dedkov et al. 2003). Perhaps, the high IHC expression of MyoD and myogenin as evaluated in the Saline group for the current study can be attributed to the Saline group undergoing a similar cycle degeneration and regeneration of muscle fibers as seen in aged animals and denervated myofibers.

In future experiments it would be important to evaluate the expression of MyoD and myogenin 1 day after reperfusion. Rabinovsky et al. 2002 showed via IHC, that IGF-I transgenic mice showed peak expression of both MRFs 1 day after nerve crush mediated injury. The levels of the MRFs gradually declined with time. In the wild type controls, MyoD expression peaked only at 3 days post injury, whereas myogenin expression started to increase at 5 days post injury. The analysis of expression levels at 14 days was not carried out but one can hypothesize that while the MyoD and myogenin levels declined in the IGF-I transgenic group, they remained elevated in the wild type group at that time point.

Desmin analysis of percent healthy fibers showed that at 4 days of reperfusion, there was no significant difference in the percentage of damaged fibers between the PEG-Fib and PEG-Fib-IGF-I treatment groups. However at 14 days post reperfusion, the PEG-Fib-IGF-I group showed a larger percentage of undamaged, viable fibers that were desmin positive. There was approximately a 37% increase in the quantity of viable fibers present in the PEG-Fib-IGF group at 14 days than at 4 days. Although, this does not confirm whether the effect of IGF-I was pro-regenerative or prevented degeneration or both, it can be stated that the IGF-I delivered via PEGylated fibrin, functions towards the maintenance of viable healthy myofibers, post I/R mediated injury. In the 14 day saline group, the ~70% myofibers that appeared to be necrotic showed minimal desmin immunoreactivity (Fig. 6A,B).

In the saline group at 14 days post I/R, it was seen that the muscle structure was still abnormal, with the tissue sections showing small muscle fibers expressing neonatal myosin heavy chain as well as large necrotic fibers. This trend also obtained via IHC, was

seen in a study by Viganud et al. 2010 in mice post I/R. The PEG-FIB-IGF group however showed very little presence of neonatal myosin positive fibers at 14 days. In fact the expression of neonatal myosin significantly decreased from 4 days to 14 days after I/R suggesting that the newly regenerated fibers had reached maturity. Our results supplement the functional data obtained by Hammers et al. (unpublished) (Fig. 1) which further demonstrates that I/R injury in rats induces detrimental effects in skeletal muscle and that the recovery following I/R injury was delayed in the saline group and PEG-Fib groups compared to the PEG-Fib-IGF-I group.

A Western Blot was performed by Hammers et al. 2011 (unpublished) on 4 day I/R recovery muscle obtained from the PEG-Fib and PEG-Fib-IGF group, to determine the signaling events involved in the action of IGF-I in skeletal muscle repair. The results are shown in Fig. 12 and indicate that the benefits of PEG-Fib-IGF may be mediated via the IGF-I induced activation of PI3K/Akt pathway. Thus, the results from this study may lead to further investigations to evaluate the effectiveness of PEG-Fib-IGF treatment in models of muscle injury. Additional studies could potentially utilize PEGylated fibrin as a delivery mechanism for combinations of growth factors and/or stem cells to enhance the process of skeletal muscle repair.

Defect Study

Studies conducted by Merritt et al. in 2010, which first employed the defect model infusing bone marrow derived stem cell (BMSC) into ECM implants as a therapeutic strategy, showed a recovery in function of the treated muscle. The addition of BMSCs to the ECM implant in the LGAS increased the number of regenerating myofibers and blood vessels throughout the defect area. The increase in blood supply and myofibers in the implant within the defect muscle is likely the reason for the partial restoration of function observed after 42 days of recovery.

The neurotization of the ECM during implantation by the transplantation of a nerve to the ECM is likely to vastly improve function (Dhawan et al. 2007). Hence Tierney et al. 2009 (thesis, unpublished), selected the peroneal nerve relocation to the ECM as an additional therapeutic modality in the defect model. The Nerve relocation (Nerve) group and the BMSC injection+Nerve group showed a significant increase in specific tension over

the ECM only group (Fig. 2). In this study, while BMSC injection was shown to be capable of improving the repopulation of desmin positive, centrally nucleated myofibers in the top and bottom regions of the ECM implant, the middle region remained relatively acellular. The dimensions of the ECM may prove to be diffusionally limiting to the paracrine factors secreted by the BMSCs, to which one can attribute the low cellular content in the middle region of the implant. The lasting relocation of the peroneal nerve alone did restore a significant amount of myofiber tissue to the top, middle and bottom region of the implant. Similarly, at least one other region in each of the two other groups that received nerve relocation (BMSC+Nerve and ADSC+Nerve), showed a significant increase in desmin positive newly regenerated myofibers, compared to the ECM only group (MATRIX). Additionally, an analysis to determine the blood vessel density within the ECM area showed that the middle region of the ECM that received the BMSC+Nerve relocation therapy showed a significantly higher vascularization than the Matrix group. This IHC data supports the higher specific tension recorded from the muscles treated with the BMSC+Nerve relocation therapy.

Carlson and Faulkner, 1996 & 1998 showed that with denervation of the muscle, although new myotubes form, there is no rapid growth or restoration of function. In a model such as the defect, there is surely a loss of nerves accompanying the fiber loss. It is important for new nerves to invade the ECM implant and form new motor endplates with the new muscle to make a functional connection to the peroneal nerve that has been relocated. In addition, the presentation of neurotrophins has been shown to regulate skeletal muscle regeneration, especially neural growth factor (NGF) from the sympathetic neurons in the peroneal nerve, may have aided in the regeneration of skeletal muscle fibers within the ECM area. This treatment showed greater potency and diffusion capacity than mesenchymal stem cell injection alone. It has been seen that electrical stimulation is capable of increasing the expression of desmin, myosin heavy chain and other myogenic factors because it is thought to mimic neuronal activity, thereby enhacing myotube formation and contractile force (reviewed in Turner and Badylak, 2011). Perhaps electrical stimulation to the defect area could be a future therapeutic strategy employed in this model of injury.

A limiting factor in the repair of skeletal muscle in this type of injury model is the

provision of nutrients and oxygen to the myoblasts. Myoblasts are unable to proliferate if a nearby source of essential nutrients and oxygen supply is not present. Promotion of angiogenesis is therefore one of the key mediators for stimulating the repair of volumetric muscle injuries. The effect of vascular endothelial growth factor (VEGF) and other angiogenic factors could be considered towards the restoration and maintenance of vasculature in the defect model. Thus the formation of an organized neurovascular system is important for muscle fiber maturation.

It is interesting to note that both innervation and vascularization will determine the regeneration potential of a tissue engineering system. A well-vascularized construct has been shown to enhance nerve regeneration (Hobson et al. 1997) while prolonged denervation stimulates the degeneration of the associated vasculature (Borisov et al. 2001).

Finally the importance of mechanical loading and exercise on the promotion of exercise must be emphasized. Regenerative medicine therapy must be followed by a period of mobilization to address the muscle atrophy that occurs during the period of rest, post injuries. Tension within the ECM as a result of mechanical load translates to the resident cells and in turn influences their phenotype (Bischoff 1997, Xu et al. 2009).

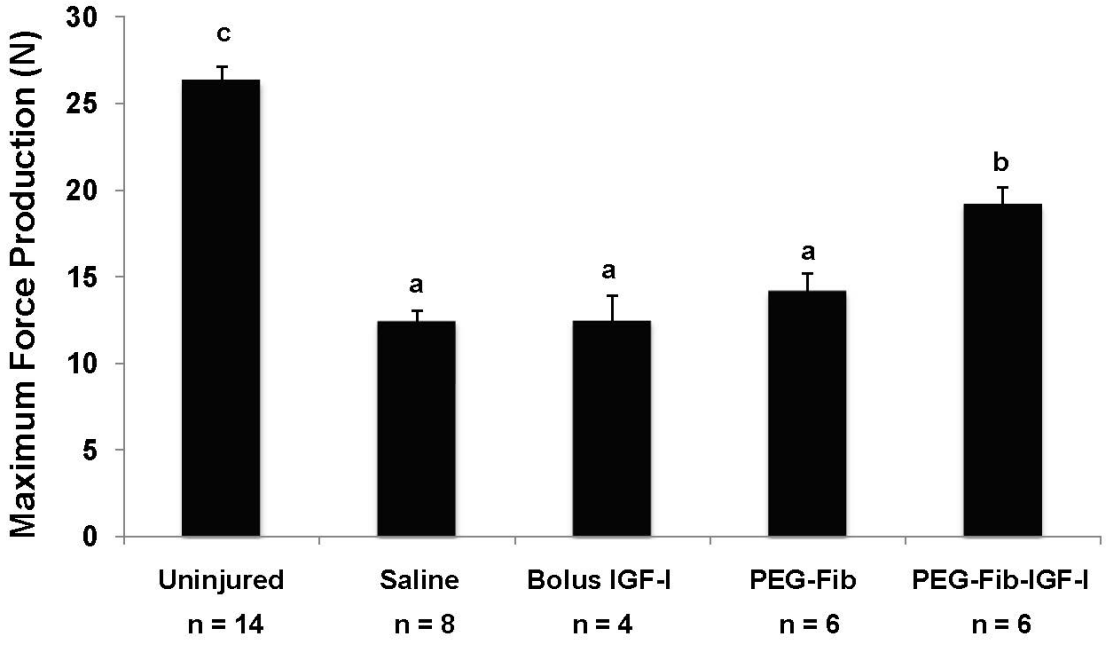

Figure 1:- Maximum force production (N) measured *in situ* at 14 days. Values obtained from the maximal isometric tetanic contraction of the lateral gastrocnemius that underwent the different treatments post TK mediated I/R. "a" represents significance from the uninjured controls labeled "c", while "b" indicates significance from all groups but the control "c". (Hammers et al. unpublished)

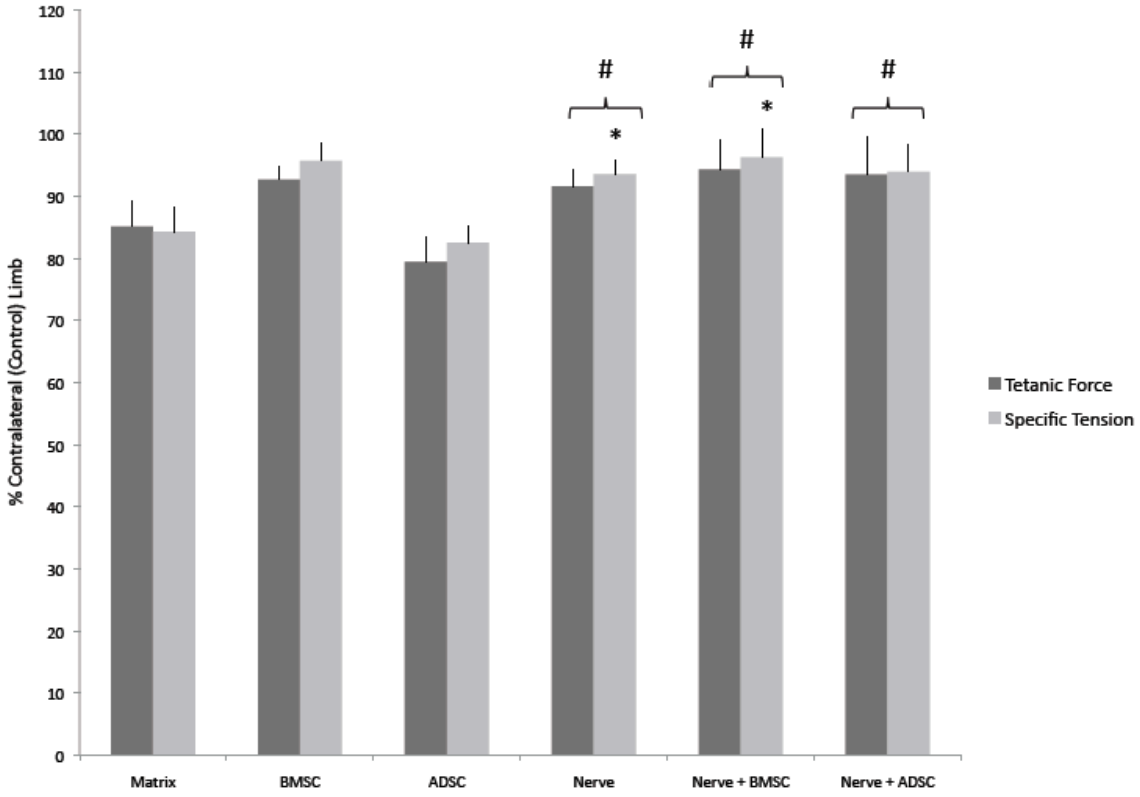

Figure 2:- Taken from Tierney et al. (unpublished). Force production (N) and Specific Tension (N/cm2) resulting from maximal isometric tetanic contraction of the lateral gastrocnemius containing the defect, 42 days post recovery. Expressed as a percentage relative to the contralateral (internal control) limb. * indicates statistical significance from the MAT group ($p<0.05$). # indicates statistical significance from the ADSC group ($p<0.05$).

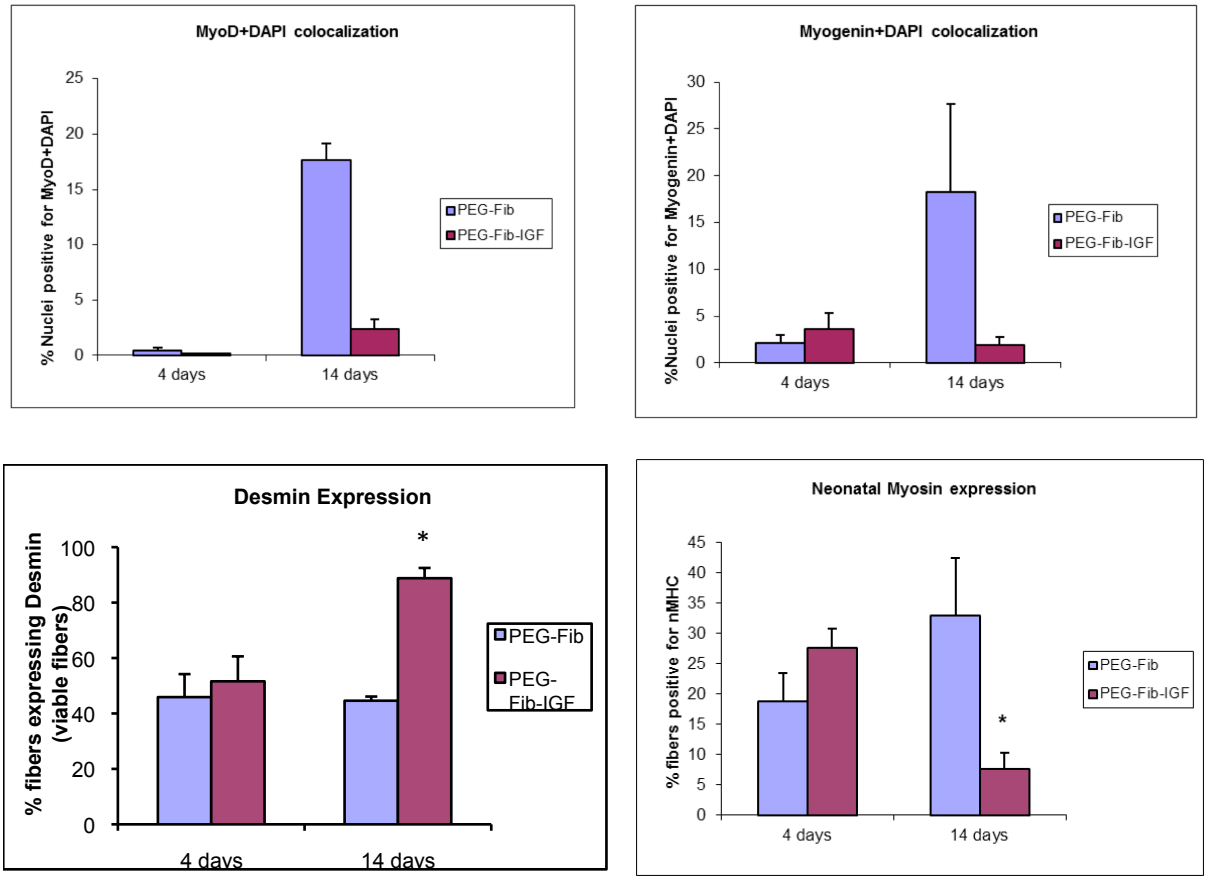

Figure 3: - Trend showing the change in MyoD, Myogenin, Desmin and neonatal myosin protein expression from 4 to 14 days in PEG-Fib and PEG-Fib-IGF-I groups. * indicates significance from mean seen at 4 days within the same group. All values are expressed as a percentage mean±SEM obtained from n=3 animals.

A.

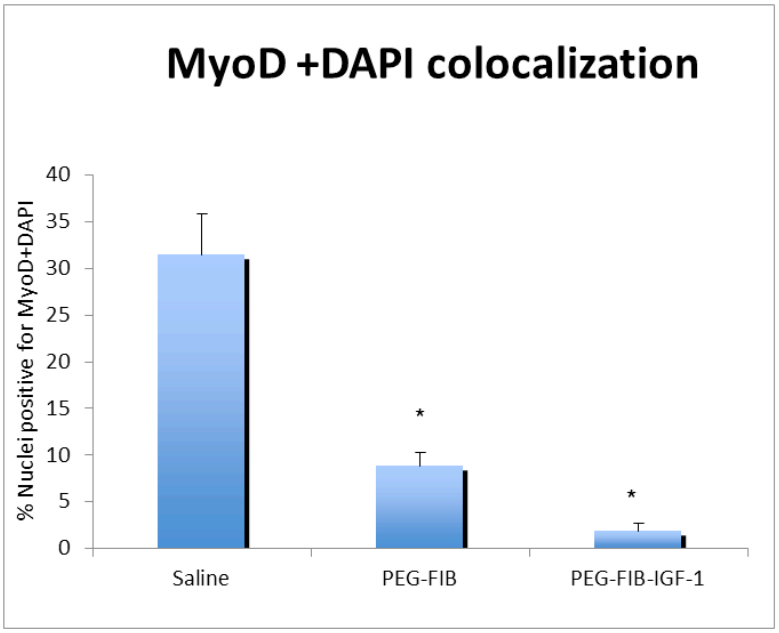

B. Saline PEG-Fib PEG-Fib-IGF-I

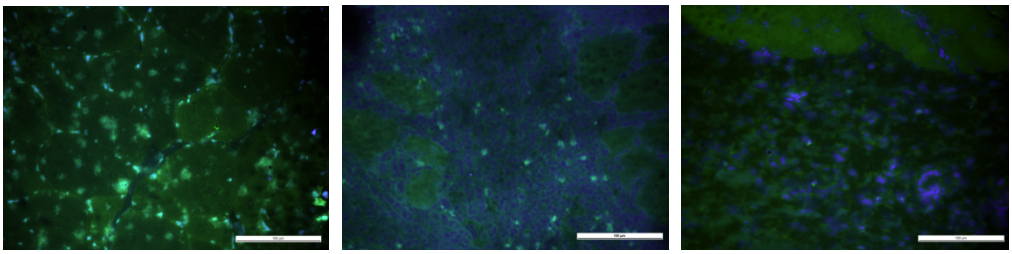

Figure 4:- A). Immunohistochemical quantification of nuclei co-expressing DAPI and MyoD. * indicates statistical significance from the Saline group ($p<0.05$). All values are expressed as a percentage mean±SEM obtained from n=3 animals. B) IHC group comparison of nuclear co-localization of MyoD and DAPI. Representative images of all groups shown here. Magnification 20x, Scale bar=100µm.

A.

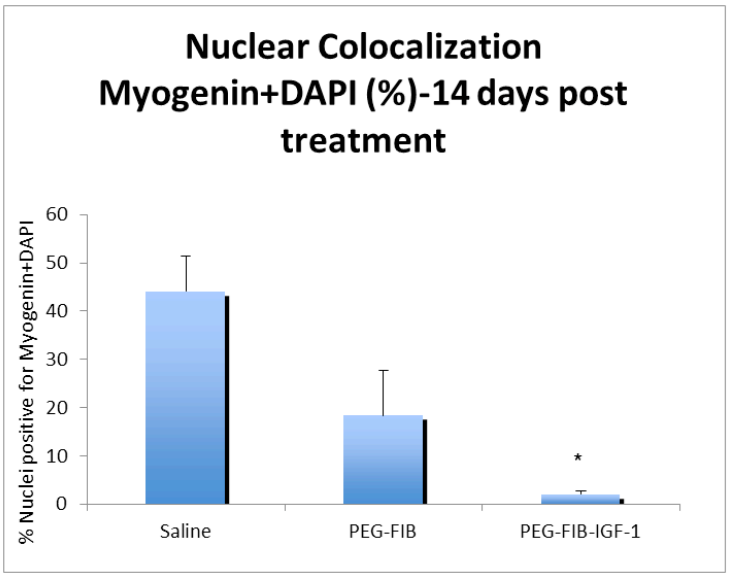

B.

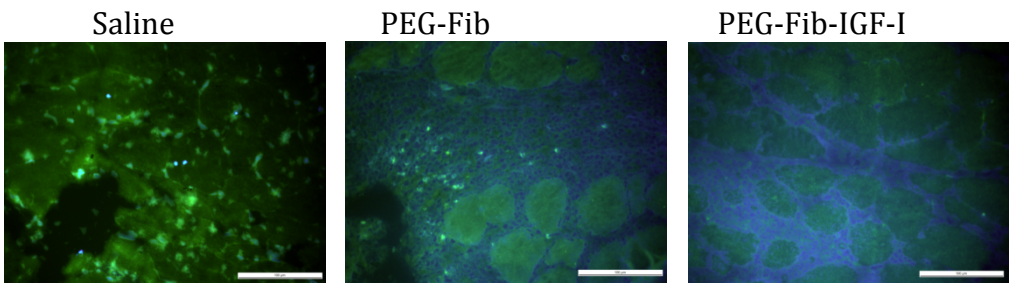

Figure 5:- A). Immunohistochemical quantification of nuclei co-expressing DAPI and Myogenin. * indicates statistical significance from the Saline group ($p<0.05$). All values are expressed as a percentage mean±SEM obtained from n=3 animals. B) IHC group comparison of nuclear co-localization of Myogenin and DAPI. Representative images of all groups shown here.
Magnification 20x, Scale bar=100µm.

A.

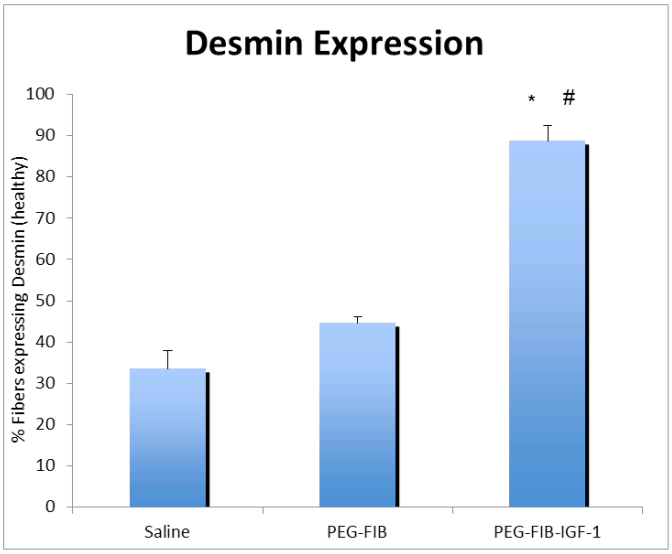

B.

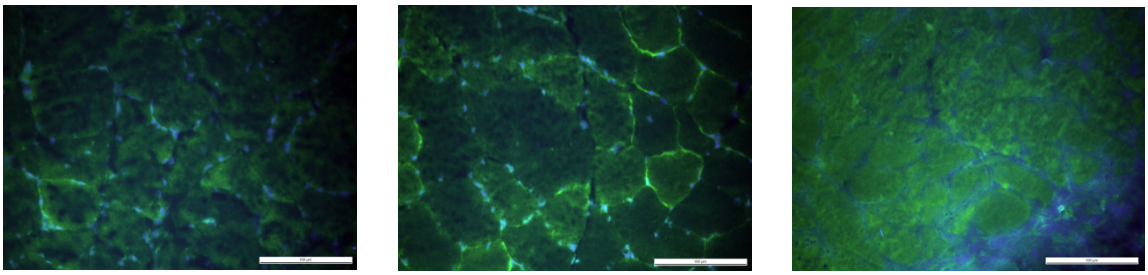

Figure 6:- A) Immunohistochemical quantification of Desmin positive fibers. * indicates significance from the Saline group, # indicates significance from the PEG-Fib group. All values are expressed as a percentage mean ± SEM obtained from n=3 animals. Magnification 20x, Scale bar=100µm.

A.

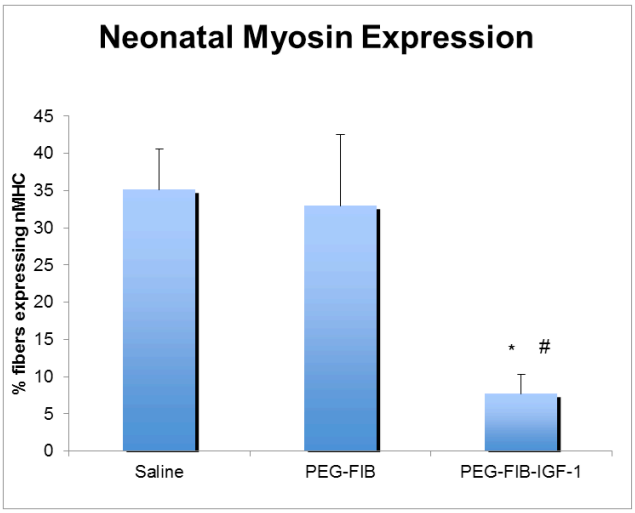

B. Saline PEG-Fib PEG-Fib-IGF-I

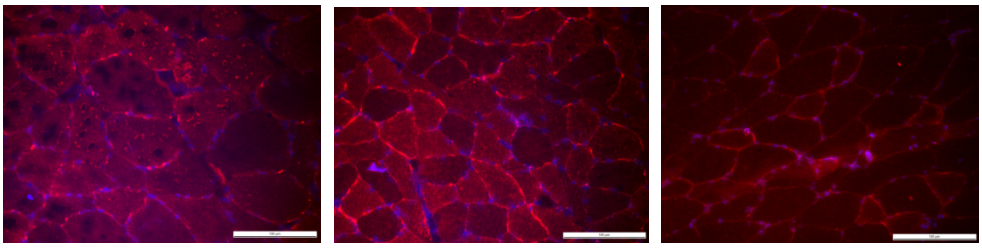

Figure 7:- A) Immunohistochemical quantification of neonatal myosin positive fibers. * indicates significance from the Saline group, # indicates significance from the PEG-Fib group. All values are expressed as a percentage mean±SEM obtained from n=3 animals. Magnification 20x, Scale bar=100µm.

A.

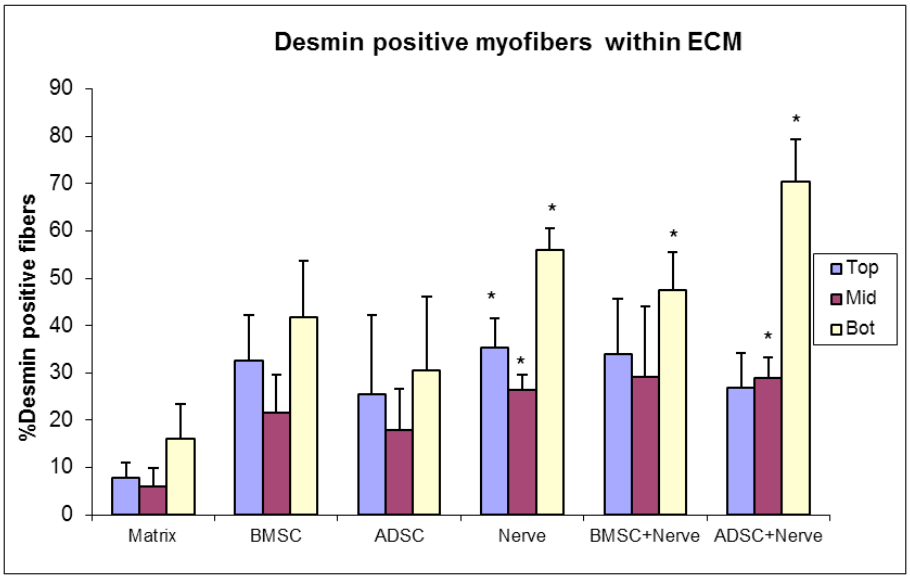

B.

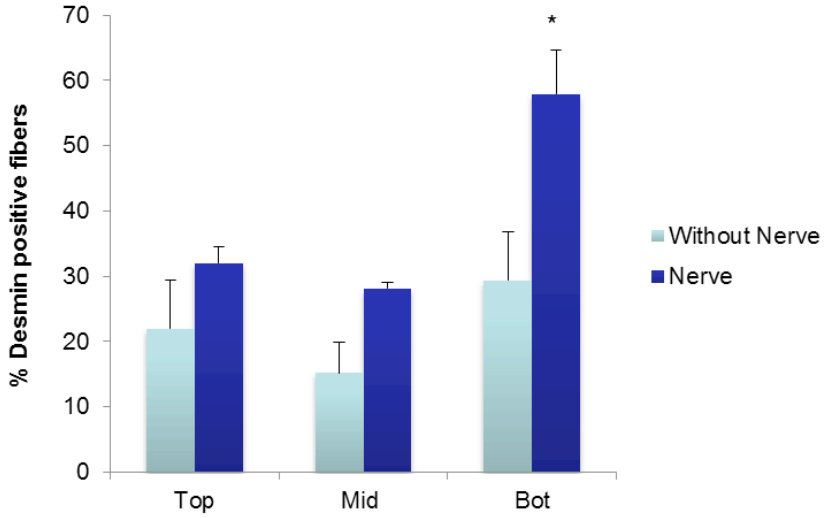

Figure 8:- A). Immunohistochemical quantification of cellular content within the top, middle and bottom regions of the defect, following 42 days recovery. * indicates statistical significance from the corresponding region of the Matrix group ($p<0.05$).
B). IHC quantification combining data across groups that did not receive peroneal nerve relocation versus groups that did receive peroneal nerve relocation. Here * indicates statistical significance from the group that did not receive nerve relocation and within the same region.

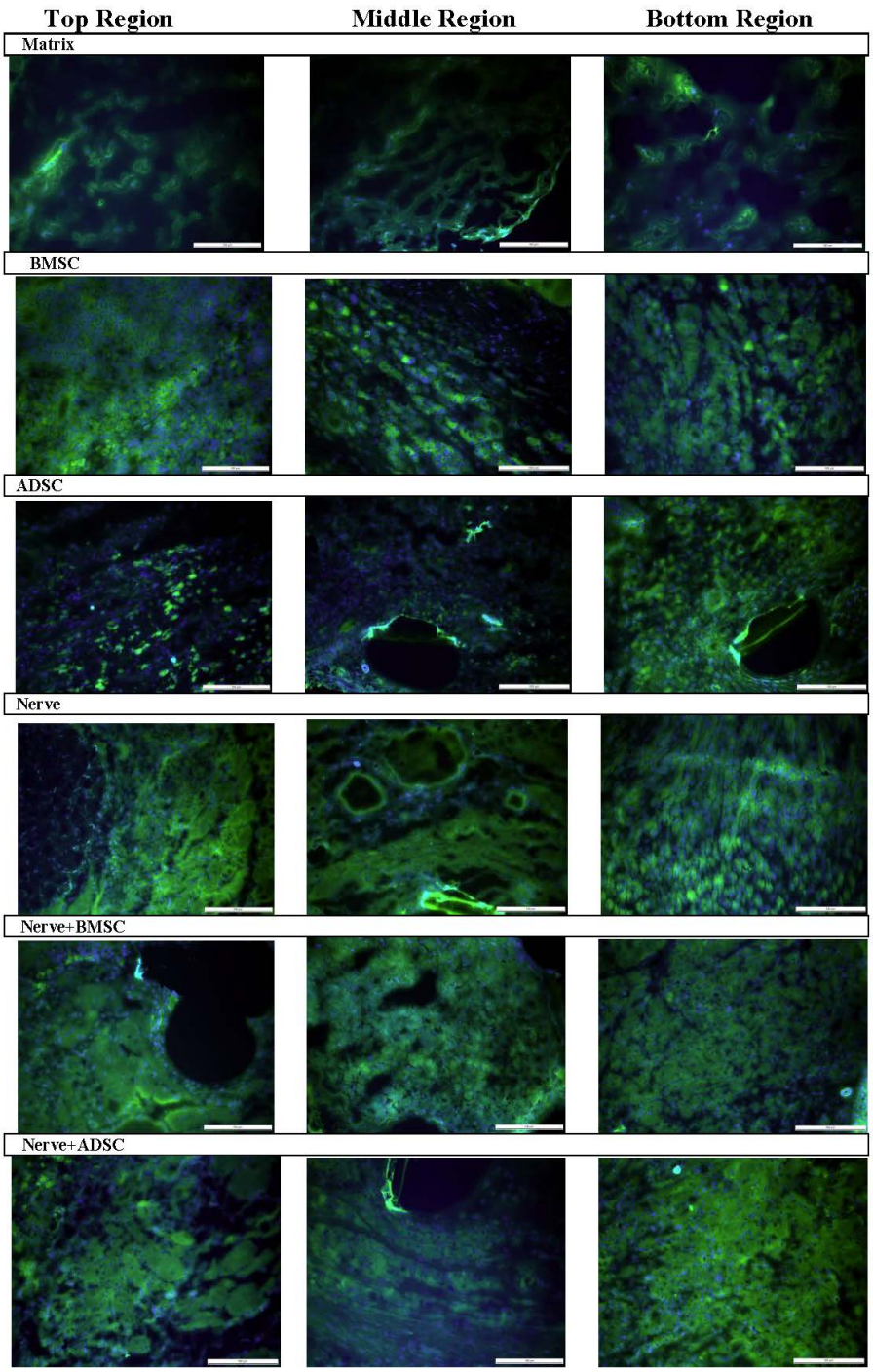

Figure 9: - Immunohistochemical identification of regenerating myofibers within the top, middle and bottom regions of the ECM. Representative images of desmin-positive structures within the implanted ECM 42 days recovery. DAPI counter stain to label nuclei. Magnification 20x. Scale bar = 100 µm.

A.

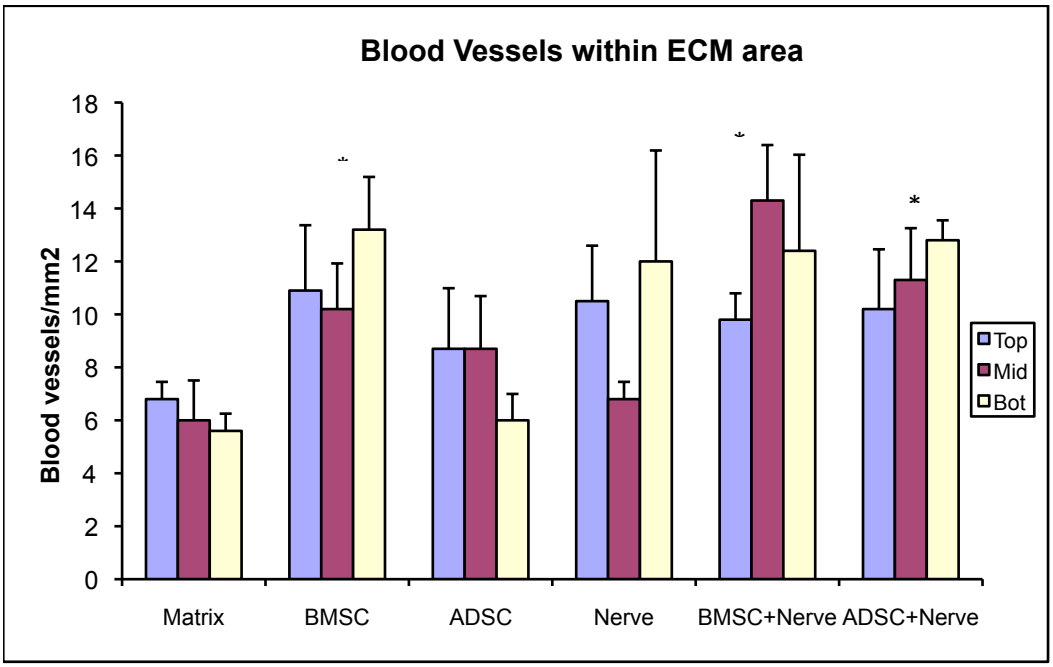

B.

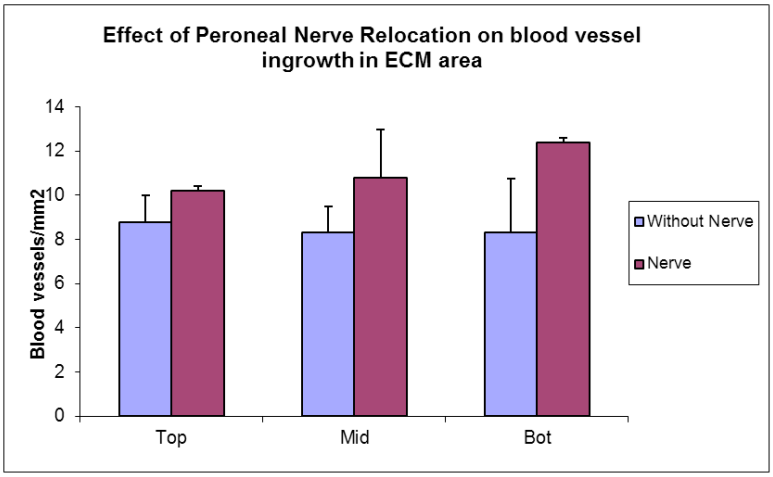

Figure 10: - A). Immunohistochemical quantification of blood vessel desnity within the top, middle and bottom regions of the defect, following 42 days recovery. * indicates statistical significance from the corresponding region of the Matrix group ($p<0.05$).
B). IHC quantification combining data across groups that did not receive peroneal nerve relocation versus groups that did receive peroneal nerve relocation. Here * indicates statistical significance ($p<0.05$) from the group that did not receive nerve relocation (within the same region).

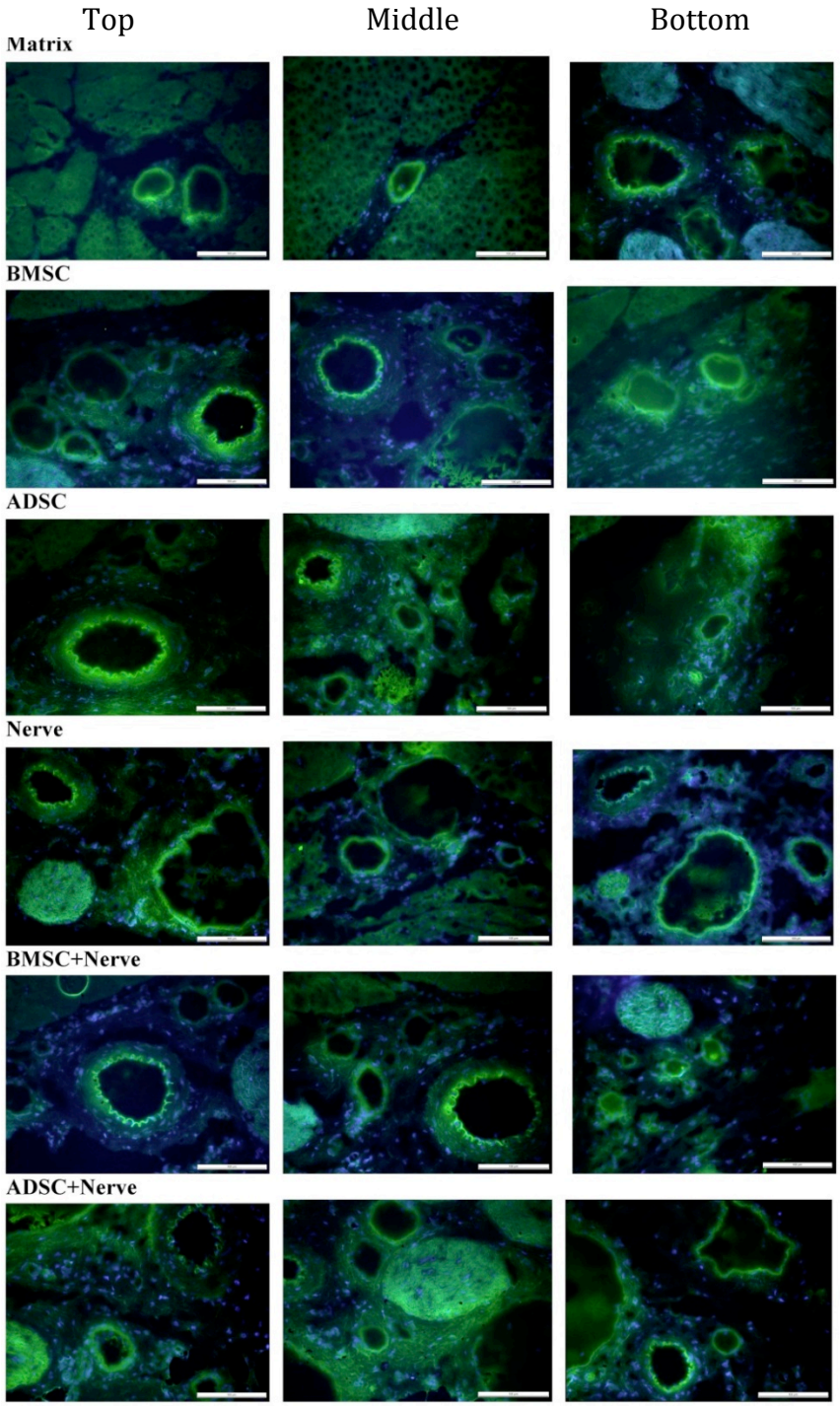

Figure 11:- Immunohistochemical identification of blood vessel density within the top, middle and bottom region of the ECM. Representative images of PECAM-1 positive structures within the implanted ECM 42 days recovery. DAPI counter stain to label nuclei. Magnification 20x. Scale bar = 100 μm.

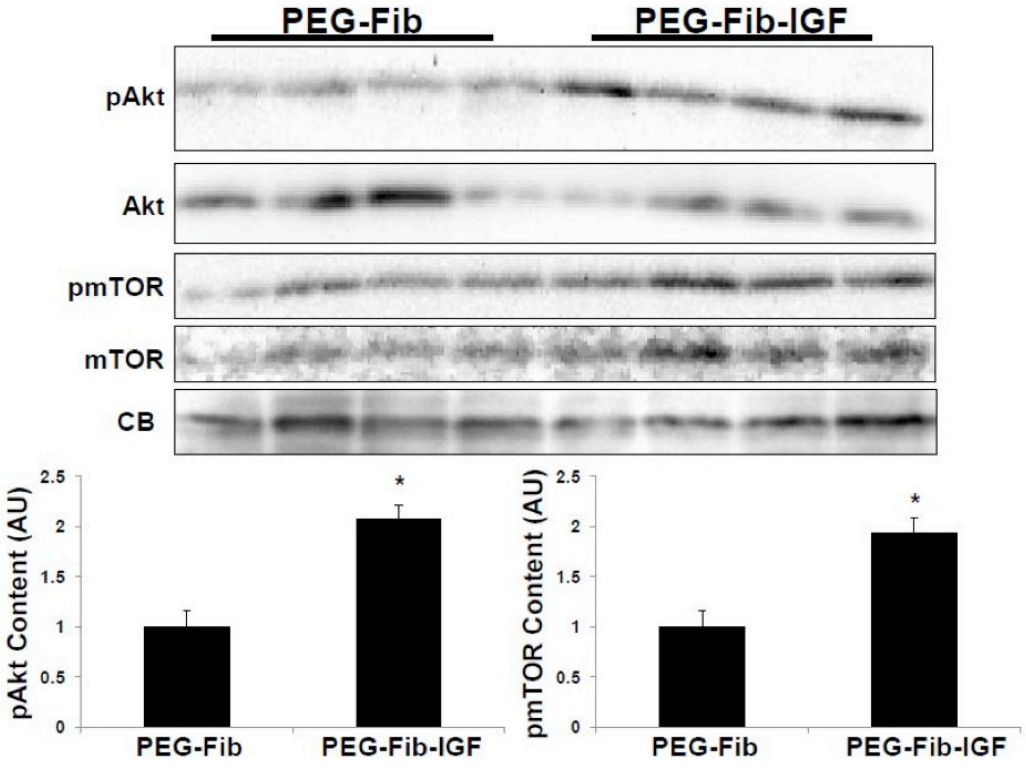

Figure 12:- Western Blot data taken from Hammers et al. (unpublished). The PEG-Fib-IGF-I treatment causes enhanced phosphorylation of Akt and mTOR, as seen in tissues post 4 days of recovery from I/R.

Appendix A: Instrumentation

1. Rapid Sectioning Cryostat: Leica CM1900, Meyer Instruments, Inc.
   The microtome blade was used to produce serial sections of frozen skeletal muscle tissue for use in immunohistochemical analysis.

2. Fluorescent Microscope: Leica DM LB2, Leica Microsystems, Inc.
   Used for magnifying and visualization of immunofluorescent structures contained within frozen tissue sections obtained from the cryostat.

3. Digital Microscope Camera: Leica DFC340FX, Leica Microsystems, Inc.
   Used for the acquisition and collection of images visualized by the Leica DM LB2 fluorescent microscope.

Appendix B: Tissue Sectioning

Cryostats contain a refrigerated compartment that has a microtome. The cryostat chamber was maintained at -22°C and 5 μm thick sections were sliced from the tissues for immunohistochemical examination. The specimen head temperature is maintained at -10 degrees Celsius.

Protocol

1. Set the specimen head temperature at -20 degrees Celsius.
2. Frozen tissue was transported from the -80°C freezer placed within the cryostat chamber.
3. Using single-edge razor blades, the portion of the tissue that is important for analysis is cut off before mounting onto specimen disks for sectioning.
4. Mount tissue onto specimen disks using optimal cutting temperature compound (OCT).
5. Insert specimen disk into specimen head and orient specimen head if necessary.
6. Initially adjust base of the blade holder to bring blade close to tissue using coarse feed settings and handwheel.
7. Begin sectioning tissue; ensuring sections are sliding under the anti-roll plate.
8. Gently place sectioned tissue from blade holder using a microscope slide; two tissue sections are placed on each microscope slide.
9. Appropriately label microscope slide and place in slide holder for future use.

Appendix C: Immunohistochemical analysis

Immunohistochemistry is a technique that detects the presence of a specific protein on a tissue section, by binding to it a primary antibody, which is in turn recognized by a secondary antibody conjugated to a fluorophore. For both studies of skeletal muscle injury, expression of select primary proteins was evaluated by using either fluorescein- or rhodamine-conjugated secondary antibodies. Each emits at different wavelengths, fluorescein at 495 nm and rhodamine at 570 nm. Additionally, tissue sections were incubated with DAPI as it emits at 461 nm. These different excitation wavelengths allowed us to separately image all proteins and overlay those images, creating a composite image spatially locating all three proteins.

Blocking agents used were bovine serum albumin (BSA) and normal donkey serum derived from the source of the primary antibody were used to inhibit non-specific binding of antibodies during staining procedures. Additionally, BSA served to stabilize enzymes and enzymatic reactions while preventing adhesion of enzymes to equipment surfaces.

<u>Protocol</u>

1. Fix slides with cold acetone (stored in the -4°C chest freezer) for 7 to 8 mins at room temperature
    a. Wash with 1X PBS, 3 times (each 5 mins)
    b. Let it dry until there are no droplets left for ~10 mins
    c. Blot off excess droplets on the sides with Kimwipe
2. Put slides in humid box (wet paper towel at the bottom of the box).
3. Circle the specimens with the barrier pen and allow ~ 5 mins to dry
4. With a dropper add, 5% donkey serum diluted with 1X PBS & 1% BSA
    a. Cover the humid box and leave at room temperature for 2 hours
    b. Let sections dry for ~10 mins (slant slides against the wall)
    c. Blot off excess droplets on the sides w/Kimwipe.

5. 1º Antibody
    a. For PECAM, use 2% (1: 50 dilution). For all other Primary antibodies namely, Desmin, MyoD, Myogenin and Neonatal myosin a 1:200 dilution is used. All antibodies are diluted in 1X PBS & 1% BSA & 5% donkey serum.
    b. Leave overnight in the humid box in 4ºC fridge (~12 hours)
    c. Wash with 1X PBS 3 times (each 5 mins)
    d. Let sections dry until there are no droplets left for ~10 mins
    e. Blot off excess droplets on the sides w/Kimwipe
6. 2º Antibody → DO THIS IN THE DARK
    a. 1% of 2º Antibody is diluted in 1% BSA & 5% donkey serum and applied to the tissue sections before incubation in the humid boxes.
    b. Put foil over the top of the humid boxes.
    c. Leave slides in the dark in the 4ºC fridge for 1.5 hours
    d. Thaw the DAPI for 45 mins for the counterstain at room temperature. DAPI is stored in the -20ºC freezer when not in use.
    e. Wash slides with 1X PBS 3 times (each 5 mins)
    f. Let sections dry for ~10 mins (slant slides against the wall)
    g. Blot off excess droplets on the sides w/Kimwipe
7. DAPI (counterstain) → DO THIS IN THE DARK
    a. Apply 1µL of DAPI + 1mL of 1X PBS to the sections for ~12 to 15 mins
    b. Wash with 1X PBS 3 times (each 5 mins)
    c. Let it dry for ~30 mins to an hour (slant slides against the wall)
    d. Mount the slides w/Permount and let dry for ~30 mins to an hour.

Appendix D: Raw Data

PEG-Fib only: 4day I/R recovery group

	# of MyoD+DAPI nuclei	Area occ.by one nucleus(sq.inches)	Total area of all nuclei(sq.inches)	%nuc.colocalization
3_PEG20401	1	0.054	37.693	0.143262675
4_PEG20401	0	NA	NA	0
5_PEG20401	0	NA	NA	0
AVG				**0.047754225**
1_PEG20403	0	NA	NA	0
2_PEG20403	1	0.089	46.814	0.190114068
4_PEG20403	2	0.055	4.345	2.53164557
AVG				**0.907253213**
2_PEG20404	0	NA	NA	0
3_PEG20404	2	0.093	17.803	1.044767736
4_PEG20404	0	NA	NA	0
AVG				**0.348255912**
Total Avg				**0.434421117**
STDEV				0.436179962
SEM				**0.251828619**

PEG-Fib-IGF : 4day I/R recovery group

Image label	#MyoD+DAPI nuclei	Area occ.by one nucleus	Total area of all nuclei(sq.inches)	%nuc.colocalization
2_IGF20401	4	0.048	110.387	0.17393352
4_IGF20401	2	0.068	41.224	0.32990491
5_IGF20401	4	0.048	121.789	0.15764971
AVG				**0.22049605**
2_IGF20402	0	NA	NA	0
3_IGF20402	2	0.042	20.903	0.40185619
5_IGF20402	0	NA	NA	0
AVG				**0.13395206**
1_IGF20403	2	0.055	106.799	0.10299722
3_IGF20403	3	0.074	100.666	0.22053126
4_IGF20403	1	0.078	62.724	0.12435431
AVG				**0.14929427**

TOTAL AVG				**0.16791413**
STDEV				0.04617889
SEM				**0.02666139**

Saline: 14 day I/R recovery group

Image Label	**#MyoD+DAPI nuclei**	**Area occ.by one nucleus**	**Total area all nuc.**	**%nuc.colocalization**
1_RS21406	25	0.061	6.344	24.0384615
2_RS21406	18	0.081	16.2	9
5_RS21406	69	0.055	9.46	40.1162791
AVG				**24.3849135**
1_RS21407	44	0.054	7.182	33.0827068
2_RS21407	32	0.049	8.036	19.5121951
3_RS21407	84	0.08	12	56
AVG				**36.1983006**
1_RS21405	96	0.051	11.118	44.0366972
2_RS21405	57	0.086	11.18	43.8461538
3_RS21405	44	0.087	29.058	13.1736527
AVG				**33.6855013**
TOTAL AVG				**31.4229051**
STDEV				6.22322541
SEM				4.40048489

PEG-Fib: 14 days I/R recovery group

Image Label	**#MyoD+DAPI nuclei**	**Area occ.by one nucleus(sq.inches)**	**Total area of all nuclei(sq.inches)**	**%nuc. colocalization**
1_PEG21404	14	0.087	76.358	1.595117735
2_PEG21404	15	0.169	118.662	2.136319968
3_PEG21404	12	0.105	10.92	11.53846154
AVG				**5.089966414**
2_PEG21405	8	0.044	5.93	5.935919056
8_PEG21405	35	0.098	91.845	3.734552779
10_PEG21405	38	0.048	141.775	1.286545583
AVG	27			**3.652339139**
1_PEG21406	16	0.085	8.585	15.84158416
2_PEG21406	22	0.033	3.828	18.96551724
3_PEG21406	15	0.08	6.64	18.07228916

AVG				**17.62646352**
TOTAL AVG				**8.789589691**
STDEV				2.650324754
SEM				**1.53016571**

PEG-Fib-IGF: 14 day recovery group

Image Label	**#MyoD+DAPI nuclei**	**Area occ. By one nucleus(sq.inches)**	**Total area of al nuclei(sq.inches)**	**%nuc.colocalization**
1_IGF21401	12	0.105	48.187	2.61481312
2_IGF21401	2	0.081	8.667	1.86915888
3_IGF21401	5	0.056	5.88	4.76190476
AVG				**3.08195892**
2_IGF21403	0	NA	NA	0
4_IGF21403	0	NA	NA	0
5_IGF21403	3	0.045	22.424	0.60203354
AVG				**0.20067785**
2_IGF21405	10	0.081	16.848	4.80769231
3_IGF21405	1	0.088	15.84	0.55555556
4_IGF21405	2	0.063	6.993	1.8018018
AVG				**2.38834989**
TOTAL AVG				1.89032888
STDEV				1.50381643
SEM				0.86822882

PEG-Fib: 4day I/R recovery group

Image Label	# Myogenin+DAPI nuclei	Area occ.by one nucleus (sq.in.)	Total area of all nuc.	%Nuc. colocalization
1_PEG20401	5	0.038	22.073	0.860780139
3_PEG20401	3	0.041	47.316	0.259954349
5_PEG20401	3	0.054	7.614	2.127659574
AVG				**1.082798021**
1_PEG20403	2	0.042	3.906	2.150537634
5_PEG20403	1	0.038	5.32	0.714285714
6_PEG20403	1	0.036	4.428	0.81300813
AVG				**1.225943826**
1_PEG20404	6	0.057	7.524	4.545454545
2_PEG20404	8	0.081	26.697	2.427239016
3_PEG20404	5	0.045	4.725	4.761904762
AVG				**3.911532774**
STDEV				1.59345636
SEM				**0.919982458**
TOT AVG				**2.073424874**

PEG-Fib-IGF: 4 day I/R recovery group

Image Label	# Myogenin+DAPI nuclei	Area occ.by one nucleus (sq.in.)	Total area of all nuc.	%Nuc.colocalization
1_IGF20401	21	0.092	72.758	2.6553781
2_IGF20401	20	0.063	87.268	1.44382821
3_IGF20401	11	0.069	14.076	5.39215686
AVG				**3.16378772**
1_IGF20402	8	0.058	106.758	0.43462785
2_IGF20402	14	0.044	105.74	0.582561
3_IGF20402	12	0.046	37.897	1.45657968
AVG				**0.82458951**
1_IGF20403	21	0.074	39.081	3.9763568
2_IGF20403	21	0.076	11.248	14.1891892
3_IGF20403	15	0.131	88.257	2.22645229
AVG				**6.79733276**
STDEV				3.00965557
SEM				**1.73762545**

TOT AVG				**3.59523666**

Saline: 14 day I/R recovery group

Image Label	**# Myogenin+DAPI nuclei**	**Area occ.by one nucleus(sq.in.)**	**Total area of all nuc.**	**%Nuc.colocalization**
1_RS21406	95	0.093	15.996	55.2325581
2_RS21406	80	0.045	6.12	58.8235294
3_RS21406	90	0.074	12.58	52.9411765
AVG				**55.6657547**
1_RS21407	58	0.099	17.919	32.0441989
2_RS21407	27	0.092	13.984	17.7631579
3_RS21407	86	0.052	7.904	56.5789474
AVG				**35.4621014**
1_RS21405	103	0.051	8.007	65.6050955
2_RS21405	66	0.082	17.302	31.2796209
3_RS21405	67	0.08	20.16	26.5873016
AVG				**41.1573393**
TOTAL AVG				**44.0950651**
STDEV				10.417273
SEM				**7.36612436**

PEG-Fib: 14 day I/R recovery group

Image Label	**#Myogenin+DAPI nuclei**	**Area occ.by one nucleus(sq.in.)**	**Total area of all nuc.**	**%Nuc.colocalization**
1_PEG21404	19	0.059	8.496	13.19444444
2_PEG21404	25	0.103	38.333	6.717449717
3_PEG21404	74	0.075	15	37
AVG				**18.97063139**
1_PEG21405	51	0.046	158.004	1.484772537
2_PEG21405	19	0.082	75.558	2.061992112
4_PEG21405	23	0.052	75.94	1.574927574
AVG				**1.707230741**
1_PEG21406	39	0.084	11.172	29.32330827
2_PEG21406	46	0.065	11.05	27.05882353
3_PEG21406	60	0.061	7.869	46.51162791
AVG				**34.2979199**

TOTAL AVG				**18.32526068**
STDEV				16.30492663
SEM				**9.413653781**

PEG-Fib-IGF: 14 day I/R recovery group

Image Label	**# of nuclei**	**Area occ.by one nucleus (sq.in.)**	**Total area of all nuc.**	**%Nuc.colocalization**
1_IGF21401	5	0.08	34.562	1.15734043
2_IGF21401	3	0.047	6.345	2.22222222
3_IGF21401	8	0.076	8.132	7.47663551
AVG				**3.61873272**
2_IGF21403	4	0.067	141.884	0.1888867
3_IGF21403	8	0.067	24.409	2.19591134
4_IGF21403	2	0.036	3.492	2.06185567
AVG				**1.4822179**
1_IGF21405	0	NA	NA	0
2_IGF20405	3	0.082	20.91	1.17647059
3_IGF20405	8	0.052	35.325	1.17763623
AVG				**0.78470227**
TOTAL AVG				**1.9618843**
STDEV				1.47664892
SEM				**0.85254365**

PEG-Fib: 4 day I/R recovery group

Image Label	**# of Desmin positive fibers**	**Total # fibers**	**%Healthy fibers**
1_PEG20401	26	51	50.98039216
2_PEG20401	15	59	25.42372881
3_PEG20401	24	49	48.97959184
AVG			**41.79457094**
2_PEG20403	4	35	11.42857143
3_PEG20403	23	41	56.09756098

4_PEG20403	13	38	34.21052632
AVG			**33.91221957**
1_PEG20404	20	43	46.51162791
2_PEG20404	24	41	58.53658537
3_PEG20404	29	36	80.55555556
AVG			**61.86792294**
STDEV			14.41406879
SEM			**8.321966497**
Total Avg			**45.85823782**

PEG-Fib-IGF: 4 day I/R recovery group

Image Label	**# of Desmin positive fibers**	**Total# fibers**	**%Healthy fibers**
1_IGF20401	38	46	82.60869565
2_IGF20401	30	40	75
3_IGF20401	20	39	51.28205128
AVG			**69.63024898**
1_IGF20402	25	50	50
2_IGF20402	13	40	32.5
3_IGF20402	14	32	43.75
AVG			**42.08333333**
1_IGF20403	26	47	55.31914894
2_IGF20403	17	37	45.94594595
3_IGF20403	14	50	28
AVG			**43.08836496**
STDEV			15.62217578
SEM			**9.019467394**
Total Avg			**51.60064909**

Saline: 14 day I/R recovery group

Image Label	**# of Desmin positive fibers**	**Total#fibers**	**%Healthy fibers**
1_RS21406	28	66	42.4242424
2_RS21406	24	62	38.7096774
3_RS21406	21	69	30.4347826
AVG			**37.1895675**
1_RS21407	1	31	3.22580645
2_RS21407	14	48	29.1666667

3_RS21407	15	37	40.5405405
AVG			**24.3110046**
1_RS21405	12	48	25
2_RS21405	15	33	45.4545455
3_RS21405	23	50	46
AVG			**38.8181818**
TOTAL AVG			**33.4395846**
STDEV			7.94741006
SEM			**4.58843934**

PEG-Fib: 14 day I/R recovery group

Image Label	**# of Desmin positive fibers**	**Total# fibers**	**%Healthy fibers**
1_PEG21404	4	29	13.79310345
2_PEG21404	12	25	48
3_PEG21404	28	43	65.11627907
AVG			**42.30312751**
1_PEG21405	30	53	56.60377358
2_PEG21405	5	27	18.51851852
3_PEG21405	33	58	56.89655172
AVG			**44.00628128**
1_PEG21406	20	42	47.61904762
2_PEG21406	17	38	44.73684211
3_PEG21406	16	32	50
AVG			**47.45196324**
TOTAL AVG			**44.58712401**
STDEV			2.623101421
SEM			**1.514448312**

PEG-Fib-IGF: 14 day I/R recovery group

Image Label	**# of Desmin positive fibers**	**Total#fibers**	**%Healthy fibers**
1_IGF21401	40	52	76.92307692
2_IGF21401	39	50	78
3_IGF21401	36	38	94.73684211
AVG			**83.21997301**
1_IGF21403	48	51	94.11764706

2_IGF21403	51	52	98.07692308
3_IGF21403	38	40	95
AVG			**95.73152338**
1_IGF21405	50	50	100
2_IGF20405	34	53	64.1509434
3_IGF20405	47	48	97.91666667
AVG			**87.35587002**
TOTAL AVG			**88.76912214**
STDEV			6.374377171
SEM			**3.680248375**

PEG-Fib: 4 day I/R recovery group

Image Label	#Fibers expressing neonatal myosin	Total#Fibers	%Fibers expressing nMHC
1_PEG20401	7	69	10.1449275
2_PEG20401	15	59	25.4237288
3_PEG20401	17	54	31.4814815
AVG			**22.3500459**
1_PEG20403	27	56	48.2142857
2_PEG20403	8	45	17.7777778
3_PEG20403	3	40	7.5
AVG			**24.4973545**
1_PEG20404	3	32	9.375
2_PEG20404	5	36	13.8888889
3_PEG20404	2	37	5.40540541
AVG			**9.55643143**
TOT AVG			**18.8012773**
STDEV			8.07794001
SEM			**4.66380084**

PEG-Fib-IGF: 4 day I/R recovery group

Image Label	#Fibers expressing neonatal myosin	Total#Fibers	%Fibers expressing nMHC
1_IGF20401	14	48	29.1666667
2_IGF20401	13	48	27.0833333
3_IGF20401	23	54	42.5925926
AVG			**32.9475309**
1_IGF20402	16	60	26.6666667
2_IGF20402	10	52	19.2307692
3_IGF20402	10	48	20.8333333
AVG			**22.2435897**
1_IGF20403	22	62	35.483871
2_IGF20403	8	34	23.5294118
3_IGF20403	12	50	24
AVG			**27.6710942**
TOT AVG			**27.6207383**
STDEV			5.35214823
SEM			**3.09006422**

Saline: 14 day I/R recovery group

Image Label	#Fibers expressing neonatal myosin	Total#Fibers	%Fibers expressing nMHC
1_RS21406	14	56	25
3_RS21406	15	51	29.4117647
4_RS21406	8	33	24.2424242
AVG			**26.218063**
1_RS21407	24	47	51.0638298
2_RS21407	9	44	20.4545455
3_RS21407	12	39	30.7692308
AVG			**34.0958687**
1_RS21405	16	53	30.1886792
2_RS21405	30	50	60
3_RS21405	22	49	44.8979592
AVG			**45.0288795**
TOTAL AVG			**35.1142704**
STDEV			9.4466693
SEM			**5.45403706**

PEG-Fib: 14 day I/R recovery group

Image Label	#Fibers expressing neonatal myosin	Total#Fibers	%Fibers expressing nMHC
1_PEG21404	32	56	57.1428571
2_PEG21404	29	64	45.3125
3_PEG21404	29	54	53.7037037
AVG			**52.0530203**
1_PEG21405	13	46	28.2608696
2_PEG21405	9	53	16.9811321
3_PEG21405	13	50	26
AVG			**23.7473339**
1_PEG21406	7	38	18.4210526
2_PEG21406	10	36	27.7777778
3_PEG21406	6	26	23.0769231
AVG			**23.0919178**
TOTAL AVG			**32.9640907**
STDEV			16.5347458
SEM			**9.54633993**

PEG-Fib-IGF: 14 day I/R recovery group

Image Label	#Fibers expressing neonatal myosin	Total#Fibers	%Fibers expressing nMHC
1_IGF21401	5	37	13.5135135
2_IGF21401	2	49	4.08163265
3_IGF21401	0	37	0
AVG			**5.86504872**
1_IGF21403	3	50	6
2_IGF21403	8	48	16.6666667
3_IGF21403	9	56	16.0714286
AVG			**12.9126984**
1_IGF21405	1	62	1.61290323
2_IGF21405	2	57	3.50877193
3_IGF21405	4	52	7.69230769
AVG			**4.27132762**
TOTAL AVG			**7.68302492**
STDEV			4.59859766
SEM			**2.65500159**

Desmin positive fibers within ECM area: 42 days recovery

		Defect: Muscle (%)			**Average: Muscle (%)**		
Animal	Image	Top	Mid	Bot	Top	Mid	Bot
Matrix							
M030	1	2.24	4.71	3.58	6.816667	2.183333	6.833333
	2	8.51	1.84	14.33			
	3	9.7	0	2.59			
M031	1	3.237	2.96	75.196	3.089	2.037667	30.79267
	2	4.043	1.582	2.039			
	3	1.987	1.571	15.143			
M033	1	16	16.36	6.03	13.94	13.84333	10.66
	2	5.02	10.19	14.21			
	3	20.8	14.98	11.74			
Avg:					**7.948556**	**6.021444**	**16.09533**
STDEV					**5.513341**	**6.774346**	**12.87127**
SEM:					**3.183129**	**3.91117**	**7.43123**
BMSC Injection							
M021	1	16.926	18.116	14.602	18.06967	14.30867	22.20833
	2	14.991	21.094	23.176			
	3	22.292	3.716	28.847			
M058	1	41.424	20.992	68.69	28.69767	13.255	39.18333
	2	15.296	11.963	27.67			
	3	29.373	6.81	21.19			
M059	1	60.8	52.16	64.124	50.94567	37.38467	63.57133
	2	52.156	32.7	72.2			
	3	39.881	27.294	54.39			
Avg:					**32.571**	**21.64944**	**41.65433**
STDEV					**16.77677**	**13.63728**	**20.79192**
SEM:					**9.68607**	**7.873489**	**12.00422**
ADSC Injection							
M043	1	6.866	1.632	9.405	6.907	4.577	17.58933
	2	4.84	3.442	31.104			
	3	9.015	8.657	12.259			
M047	1	10.85	52.925	67.542	10.972	34.34933	61.34267
	2	14.296	22.43	51.94			
	3	7.77	27.693	64.546			
M060	1	69.293	27.089	19.99	58.74733	14.544	12.609
	2	56.143	7.904	8.29			
	3	50.806	8.639	9.547			
Avg					**25.54211**	**17.82344**	**30.51367**
STDEV					**28.8283**	**15.15467**	**26.81457**
SEM:					**16.64403**	**8.749553**	**15.4814**

Nerve Relocation		Top	Mid	Bot	Top	Mid	Bot
M025	1	15.713	21.296	65.097	23.03333	21.16967	62.44367
	2	10.296	19.223	83.386			
	3	43.091	22.99	38.848			
M027	1	18.536	28.911	72.218	44.21467	32.00167	58.27033
	2	62.334	14.304	32.82			
	3	51.774	52.79	69.773			
M028	1	68.63	39.62	79.88	38.44333	25.93667	46.83
	2	19	23.7	34.76			
	3	27.7	14.49	25.85			
Avg					**35.23044**	**26.36933**	**55.848**
STDEV					**10.95008**	**5.428946**	**8.083775**
SEM:					**6.322031**	**3.134404**	**4.66717**
BMSC+Nerve							
M041	1	14.06	47.228	10.763	24.14267	21.75533	43.691
	2	43.392	6.646	82.307			
	3	14.976	11.392	38.003			
M042	1	13.103	3.247	3.021	20.47467	57.78133	35.767
	2	24.179	79.032	6.141			
	3	24.142	91.065	98.139			
M052	1	85.349	0.8327	98.216	57.218	8.044567	62.76867
	2	32.322	11.382	62.553			
	3	53.983	11.919	27.537			
Avg:					**33.94511**	**29.19374**	**47.40889**
STDEV:					**20.23818**	**25.68918**	**13.87946**
SEM:					**11.68452**	**14.83165**	**8.013312**
ADSC+Nerve							
M039	1	17.5	11.87	78.13	23.85567	36.04667	71.599
	2	5.997	36.97	64.27			
	3	48.07	59.3	72.397			
M054	1	29.823	19.299	80.825	40.83067	20.73733	85.14933
	2	46.516	27.218	83.518			
	3	46.153	15.695	91.105			
M055	1	5.575	28.259	12.978	15.91833	29.87233	54.588
	2	5.594	10.72	64.039			
	3	36.586	50.638	86.747			
Avg:					**26.86822**	**28.88544**	**70.44544**
STDEV					**12.72646**	**7.702232**	**15.31329**
SEM:					**7.347623**	**4.446886**	**8.841131**

PECAM- positive blood vessels in the ECM area:42 days recovery

		BV Count-Image			**BV/mm2-Defect**			**BV/mm2-Defect**		
Animal	Image	Top	Mid	Bot	Top	Mid	Bot	Top	Mid	Bot
Matrix										
M030	1	3	1	2	10.15916	3.386387	6.772773	6.772773	4.515182	6.772773
	2	2	1	1	6.772773	3.386387	3.386387			
	3	1	2	3	3.386387	6.772773	10.15916			
M031	1	2	1	2	6.772773	3.386387	6.772773	7.901569	4.515182	4.515182
	2	3	2	1	10.15916	6.772773	3.386387			
	3	2	1	1	6.772773	3.386387	3.386387			
M033	1	2	3	2	6.772773	10.15916	6.772773	5.643978	9.030365	5.643978
	2	1	3	2	3.386387	10.15916	6.772773			
	3	2	2	1	6.772773	6.772773	3.386387			
Avg:								**6.772773**	**6.020243**	**5.643978**
STDEV								1.128796	2.606842	1.128796
SEM:								**0.65171**	**1.505061**	**0.65171**
BMSC Injection										
M021	1	1	4	3	3.386	13.546	16.932	7.901333	12.417	12.41667
	2	3	5	2	10.159	16.932	10.159			
	3	3	2	2	10.159	6.773	10.159			
M058	1	2	1	4	6.772773	3.386387	13.54555	9.030365	6.772773	10.15916
	2	1	3	3	3.386387	10.15916	10.15916			
	3	5	2	2	16.93193	6.772773	6.772773			

M059	1	5	3	3	16.93193	10.15916	10.15916	15.80314	11.28796	16.93193
	2	6	4	8	20.31832	13.54555	27.09109			
	3	3	3	4	10.15916	10.15916	13.54555			
Avg:								**10.91161**	**10.15924**	**13.16925**
STDEV:								4.273634	2.986606	3.448537
SEM:								**2.467384**	**1.724318**	**1.991014**
ADSC Injection										
M043	1	3	1	2	10.15916	3.386387	6.772773	9.030365	7.901569	4.515182
	2	3	4	1	10.15916	13.54555	3.386387			
	3	2	2	1	6.772773	6.772773	3.386387			
M047	1	2	1	4	6.772773	3.386387	13.54555	4.515182	5.643978	7.901569
	2	1	1	1	3.386387	3.386387	3.386387			
	3	1	3	2	3.386387	10.15916	6.772773			
M060	1	3	4	2	10.15916	13.54555	6.772773	12.41675	12.41675	5.643978
	2	3	4	1	10.15916	13.54555	3.386387			
	3	5	3	2	16.93193	10.15916	6.772773			
Avg								**8.654099**	**8.654099**	**6.020243**
STDEV								3.9642	3.448527	1.724264
SEM:								**2.288732**	**1.991008**	**0.995504**
Nerve Relocation										
M025	1	3	1	2	10.15916	3.386387	6.772773	7.901569	5.643978	9.030365
	2	2	2	4	6.772773	6.772773	13.54555			
	3	2	2	2	6.7727	6.7727	6.7727			

					73	73	73			
M027	1	3	3	3	10.15916	10.15916	10.15916	9.030365	7.901569	6.772773
	2	2	1	2	6.772773	3.386387	6.772773			
	3	3	3	1	10.15916	10.15916	3.386387			
M028	1	4	2	6	13.54555	6.772773	20.31832	14.67434	6.772773	20.31832
	2	6	3	7	20.31832	10.15916	23.70471			
	3	3	1	5	10.15916	3.386387	16.93193			
Avg:								**10.53543**	**6.772773**	**12.04049**
STDEV:								3.62857	1.128796	7.25714
SEM:								**2.094956**	**0.65171**	**4.189912**
<u>BMSC+Nerve</u>										
M041	1	5	4	4	16.93193	13.54555	13.54555	10.15916	16.93193	19.18952
	2	2	3	8	6.772773	10.15916	27.09109			
	3	2	8	5	6.772773	27.09109	16.93193			
M042	1	2	3	3	6.772773	10.15916	10.15916	7.901569	10.15916	6.772773
	2	2	4	1	6.772773	13.54555	3.386387			
	3	3	2	2	10.15916	6.772773	6.772773			
M052	1	5	4	3	16.93193	13.54555	10.15916	11.28796	15.80314	11.28796
	2	3	5	2	10.15916	16.93193	6.772773			
	3	2	5	5	6.772773	16.93193	16.93193			
Avg:								**9.782895**	**14.29808**	**12.41675**
STDEV								1.724264	3.62857	6.284868
SEM:								**0.995504**	**2.094956**	**3.62857**

ADSC+Nerve										
M039	1	2	4	4	6.772773	13.54555	13.54555	7.901569	11.28796	13.54555
	2	3	3	4	10.15916	10.15916	13.54555			
	3	2	3	4	6.772773	10.15916	13.54555			
M054	1	2	7	4	6.772773	23.70471	13.54555	7.901569	14.67434	13.54555
	2	1	3	3	3.386387	10.15916	10.15916			
	3	4	3	5	13.54555	10.15916	16.93193			
M055	1	5	2	3	16.93193	6.772773	10.15916	14.67434	7.901569	11.28796
	2	4	3	5	13.54555	10.15916	16.93193			
	3	4	2	2	13.54555	6.772773	6.772773			
Avg:								**10.15916**	**11.28796**	**12.79302**
STDEV:								3.910263	3.386387	1.303421
SEM:								**2.257591**	**1.955131**	**0.75253**

REFERENCES

Adi S, Bin-Abbas B, Wu NY, Rosenthal SM 2002. Early stimulation and late inhibition of extracellular signal-regulated kinase 1/2 phosphorylation by IGF-I: a potential mechanism mediating the switch in IGF-I action on skeletal muscle cell differentiation. *Endocrinology* 143(2): 511-6.

Allbrook D. 1981. Skeletal muscle regeneration. *Muscle Nerve*. 4(3): 234-45.

Alway SE, Lowe DA, Chen KD 2001. The effects of age and hindlimb supension on the levels of expression of the myogenic regulatory factors MyoD and myogenin in rat fast and slow skeletal muscles. *Exp Physiol.* 86(4): 509-17.

Andrés V and Walsh K 1996. Myogenin expression, cell cycle withdrawal, and phenotypic differentiation are temporally separable events that precede cell fusion upon myogenesis. *J Cell Biol*. 132(4): 657-66.

Arnold L, et al. 2007. Inflammatory monocytes recruited after skeletal muscle injury switch into antiinflammatory macrophages to support myogenesis. *J Exp Med*. 204(5): 1057–1069

Baksh D, Song L, Tuan RS 2004. Adult mesenchymal stem cells: characterization, differentiation, and application in cell and gene therapy.
J Cell Mol Med. 8(3): 301-16. Review.

Barton ER, Morris L, Musaro A, Rosenthal N, Sweeney HL 2002. Muscle-specific expression of insulin-like growth factor I counters muscle decline in mdx mice. *J Cell Biol*. 2002 Apr 1; 157(1): 137-48.

Barton-Davis ER, Shoturma DI, Sweeney HL 1999. Contribution of satellite cells to IGF-I induced hypertrophy of skeletal muscle. *Acta Physiol Scand*. 1999. 167(4): 301-5.

Beiner JM, Jokl P 2001. Muscle contusion injuries: current treatment options. *J Am Acad Orthop Surg*. 9(4): 227-37.

Bischoff R, 1997 Chemotaxis of skeletal muscle satellite cells. *Dev Dyn*. 208(4): 505-15.

Bischoff J 1997. Cell adhesion and angiogenesis. *J Clin Invest*. 100(11 Suppl):S37-9.

Bittner RE, Schöfer C, Weipoltshammer K, Ivanova S, Streubel B, Hauser E, Freilinger M, Höger H, Elbe-Bürger A, Wachtler F 1999. Recruitment of bone-marrow-derived cells by skeletal and cardiac muscle in adult dystrophic mdx mice. *Anat Embryol* (Berl). 199(5):391-6.

Bixby JL, Van Essen DC 1979. Competition between foreign and original nerves in adult mammalian skeletal muscle. *Nature.* 282(5740): 726-8.

Blaisdell FW 2002. The pathophysiology of skeletal muscle ischemia and the reperfusion syndrome: a review. *Cardiovascular Surgery* 10(6): 620-630

Bodine SC, Stitt TN, Gonzalez M, Kline WO, Stover GL, Bauerlein R, Zlotchenko E, Scrimgeour A, Lawrence JC, Glass DJ, Yancopoulos GD 2001. Akt/mTOR pathway is a crucial regulator of skeletal muscle hypertrophy and can prevent muscle atrophy in vivo. *Nat Cell Biol*. 3(11): 1014-9.

Bondensen BA, Miss ST, Kegley KM and Pavlath GK 2004. The COX-2 pathway is essential during early stages of skeletal muscle regeneration. *Amer J Physiol Cell Physiol* 287, C475-C483.

Borisov AB, Dedkov EI, Carlson BM 2001. Interrelations of myogenic response, progressive atrophy of muscle fibers, and cell death in denervated skeletal muscle. *Anat Rec*. 264(2):203-18.

Borschel GH, Dennis RG, Kuzon WM Jr. 2004. Contractile skeletal muscle tissue-engineered on an acellular scaffold. *Plast Reconstr Surg*. 113(2): 595-602; discussion 603-4.

Carlson BM, Faulkner JA 1996. The regeneration of noninnervated muscle grafts and marcaine-treated muscles in young and old rats*. J Gerontol A Biol Sci Med Sci.* 51(1): B43-9.

Carlson BM, Faulkner JA 1998. Muscle regeneration in young and old rats: effects of motor nerve transection with and without marcaine treatment. *J Gerontol A Biol Sci Med Sci.* 53(1):B52-7.

Chakravarthy MV, Davis BS, Booth FW 2000. IGF-I restores satellite cell proliferative potential in immobilized old skeletal muscle. *J Appl Physiol*. 89(4):1365-79

Charge SB and Rudnicki MA 2004. Cellular and molecular regulation of muscle regeneration. *Physiol Rev*. 84 (1): 209-38.

Conconi MT, De Coppi P, Bellini S, Zara G, Sabatti M, Marzaro M, Zanon GF, Gamba PG, Parnigotto PP, Nussdorfer GG 2005. Homologous muscle acellular matrix seeded with autologous myoblasts as a tissue-engineering approach to abdominal wall-defect repair. *Biomaterials.* 26(15): 2567-74.

Coolican SA, Samuel DS, Ewton DZ, McWade FJ, Florini JR. The mitogenic and myogenic actions of insulin-like growth factors utilize distinct signaling pathways. *J Biol Chem.* 272(10):6653-62.

Dedkov EI, Borisov AB, Carlson BM 2003. Dynamics of postdenervation atrophy of young and old skeletal muscles: differential responses of fiber types and muscle types*. J Gerontol A Biol Sci Med Sci*. 58(11):984-91.

Deponti D, Buono R, Catanzaro G, De Palma C, Longhi R, Meneveri R, Bresolin N, Bassi MT, Cossu G, Clementi E, Brunelli S. The low-affinity receptor for neurotrophins p75NTR plays a key role for satellite cell function in muscle repair acting via RhoA. *Mol Biol Cell*. 20(16): 3620-7.

Dezawa M, Ishikawa H, Itokazu Y, Yoshihara T, Hoshino M, Takeda S, Ide C, Nabeshima Y 2005. Bone marrow stromal cells generate muscle cells and repair muscle degeneration. *Science.* 309(5732):314-7.

Dhawan V, Lytle IF, Dow DE, Huang YC, Brown DL 2007. Neurotization improves contractile forces of tissue-engineered skeletal muscle. *Tissue Eng.* 13(11): 2813-21

Edwall D, Schalling M, Jennische E, Norstedt G 1989. Induction of insulin-like growth factor I messenger ribonucleic acid during regeneration of rat skeletal muscle. *Endocrinology*. 124:820-5.

Engert JC, Berglund EB, Rosenthal N 1996. Proliferation precedes differentiation in IGF-I-stimulated myogenesis. *J Cell Biol*. 1996. 135(2): 431-40.

Filvaroff EH, Ebner R, Derynck R 1994. Inhibition of myogenic differentiation in myoblasts expressing a truncated type II TGF-beta receptor. Development. 120(5): 1085-95.

Florini JR, Ewton DZ, Coolican SA 1996. Growth hormone and the insulin-like growth factor system in myogenesis. *Endocr Rev*. 17(5): 481-517.

Füchtbauer EM, Westphal H 1992. MyoD and myogenin are coexpressed in regenerating skeletal muscle of the mouse. *Dev Dyn*. 193(1): 34-9.

Fukada S, Miyagoe-Suzuki Y, Tsukihara H, Yuasa K, Higuchi S, Ono S, Tsujikawa K, Takeda S, Yamamoto H 2002. Muscle regeneration by reconstitution with bone marrow or fetal liver cells from green fluorescent protein-gene transgenic mice. *J Cell Sci*. 115(Pt 6): 1285-93.

Garrett WE Jr. 1996. *Am J Sports Med* 24:S2–8.

Gimble JM, Guilak F 2003. Differentiation potential of adipose derived adult stem (ADAS) cells. *Curr Top Dev Biol*. 58:137-60. Review.

Gomes RR Jr and Booth FW 1998. Expression of acetylcholine receptor mRNAs in atrophying and nonatrophying skeletal muscles of old rats. *J Appl Physiol*. 85(5):1903-8.

Granger DN et al. 1988. Role of xanthine oxidase and granulocytes in ischemia-reperfusion injury. *Am J Physiol*. 255(6 Pt 2): H1269-75.

Grounds MD, Garrett KL, Lai MC, Wright WE, Beilharz MW 1992. Identification of skeletal muscle precursor cells in vivo by use of MyoD1 and myogenin probes. *Cell Tissue Res*. 267(1): 99-104.

Guiducci S, Porta F, Saccardi R, Guidi S, Ibba-Manneschi L, Manetti M, Mazzanti B, Dal Pozzo S, Milia AF, Bellando-Randone S, Miniati I, Fiori G, Fontana R, Amanzi L, Braschi F, Bosi A, Matucci-Cerinic M 2010. Autologous mesenchymal stem cells foster revascularization of ischemic limbs in systemic sclerosis: a case report. *Ann Intern Med.* 153(10):650-4.

Hammers et al. (unpublished). Controlled release of IGF-I from a biodegradable matrix improves functional recovery of skeletal muscle from ischemia reperfusion.

Hammers DW, Matheny RW Jr, Sell C, Adamo ML, Walters TJ, Estep JS, Farrar RP. *Exp Gerontol.* 2010 Apr; 46(4): 265-72.

Hammers DW, Merritt EK, Matheny RW Jr, Adamo ML, Walters TJ, Estep JS, Farrar RP 2008. Functional deficits and insulin-like growth factor-I gene expression following tourniquet-induced injury of skeletal muscle in young and old rats. *J Appl Physiol*.105 (4): 1274-81.

Hara K, Yonezawa K, Kozlowski MT, Sugimoto T, Andrabi K, Weng QP, Kasuga M, Nishimoto I, Avruch J 1997. Regulation of eIF-4E BP1 phosphorylation by mTOR. *J Biol Chem*. 272(42): 26457-63.

Hill M, Goldspink G 2003. Expression and splicing of the insulin-like growth factor gene in rodent muscle is associated with muscle satellite (stem) cell activation following local tissue damage. *J Physiol* 549:409-418, 2003.

Hill M, Wernig A, Goldspink G. Muscle satellite (stem) cell activation during local tissue injury and repair. *J Anat* 203: 89-99, 2003.

Hobson MI, Brown R, Green CJ, Terenghi G 1997. Inter-relationships between angiogenesis and nerve regeneration: a histochemical study. *Br J Plast Surg.* 50(2):125-31.

Honda HM, Korge P, Weiss JN 2005. Mitochondria and ischemia/reperfusion injury: a review. *Ann NY Acad Sci*. 1047:248-58.

Huang YC, Dennis RG, Larkin L, Baar K (2005) J *Appl Physiol* 98:706–713

Huard J, Li Y, Fu FH 2002. Muscle injuries and repair: current trends in research. *J Bone Joint Surg* Am. 84-A (5): 822-32.

Hurme T, Kalimo H 1992. Activation of myogenic precursor cells after muscle injury. *Med Sci Sports Exerc*. 24(2): 197-205.
Hurme T, Kalimo H, Lehto M, Järvinen M 1991. Healing of skeletal muscle injury: an ultrastructural and immunohistochemical study. *Med Sci Sports Exerc*. 23(7): 801-10.

Jacquemin V, Butler-Browne GS, Furling D, Mouly V 2007. IL-13 mediates the recruitment of reserve cells for fusion during IGF-1-induced hypertrophy of human myotubes. *J Cell Sci*. 120(Pt 4): 670-81.

James PL, Stewart CE, Rotwein P 1996. Insulin-like growth factor binding protein-5 modulates muscle differentiation through an insulin-like growth factor-dependent mechanism. *J Cell Biol*. 133(3):683-93.

Jansen JK, Lomo T, Nicolaysen K, Westgaard RH 1973. Hyperinnervation of skeletal muscle fibers: dependence on muscle activity. *Science*. 181(99): 559-61.

Järvinen TA, Kääriäinen M, Järvinen M, Kalimo H 2000. *Curr Opin Rheumatol*. 12(2): 155-61.

Järvinen TA, Järvinen TL, Kääriäinen M, Kalimo H, Järvinen M 2005. Muscle injuries: biology and treatment. *Am J Sports Med*. 33(5): 745-64.

Jennische E, Hannson HA 1987. Regenerating skeletal muscle cells express insulin-like growth factor I, *Acta Physiol Scand* 130: 327-332, 1987.

Jennische E, Skottner A, Hansson HA 1987. Satellite cells express the trophic factor IGF-I in regenerating skeletal muscle. *Acta Physiol. Scand* 130: 327-332.

Joel S. Fish, Nancy H. McKee, William M. Kuzon, Jr. and Michael J. Plyley 1993. The effect of hypothermia on changes in isometric contractile function in skeletal muscle after tourniquet ischemia. *The Journal of Hand Surgery*. Volume 18, Issue 2, Pages 210-217

Jones NC, Fedorov YV, Rosenthal RS, Olwin BB 2001. ERK1/2 is required for myoblast proliferation but is dispensable for muscle gene expression and cell fusion. *J Cell Physiol*. 186(1): 104-15.

Kääriäinen M, Järvinen T, Järvinen M, Rantanen J, Kalimo H 2000. Relation between myofibers and connective tissue during muscle injury repair. *Scand J Med Sci Sports*. 10(6): 332-7.

Kjeldsen L, Sengeløv H, Lollike K, Nielsen MH, Borregaard N.1994. Isolation and characterization of gelatinase granules from human neutrophils. *Blood*. 83(6):1640-9.

Kochupura PV, Azeloglu EU, Kelly DJ, Doronin SV, Badylak SF, Krukenkamp IB, Cohen IS, Gaudette GR 2005. Tissue-engineered myocardial patch derived from extracellular matrix provides regional mechanical function. *Circulation*. 112(9 Suppl):I144-9

Kooijman, R. (2006). "Regulation of apoptosis by insulin-like growth factor (IGF)-I." Cytokine Growth Factor Rev **17**(4): 305-23

Kostrominova TY, Macpherson PC, Carlson BM, Goldman D 2000. Regulation of myogenin protein expression in denervated muscles from young and old rats. *Am J Physiol Regul Integr Comp Physiol.* 279(1):R179-88.

LaBarge MA, Blau HM 2002. Biological progression from adult bone marrow to mononucleate muscle stem cell to multinucleate muscle fiber in response to injury. *Cell*. 111(4): 589-601.

Ladak A, Olson J, Tredget EE, Gordon T 2011. Differentiation of mesenchymal stem cells to support peripheral nerve regeneration in a rat model. *Exp Neurol.* 228(2):242-52.

Larkin LM, Van der Meulen JH, Dennis RG, Kennedy JB 2006. Functional evaluation of nerve-skeletal muscle constructs engineered *in vitro*. *In Vitro Cell Dev Biol Anim*. 42(3-4): 75-82.

Lassar AB, Buskin JN, Lockshon D, Davis RL, Apone S, Hauschka SD, Weintraub H 1989. MyoD is a sequence-specific DNA binding protein requiring a region of myc homology to bind to the muscle creatine kinase enhancer. *Cell.* 58(5): 823-31.

Latres E, Amini AR, Amini AA, Griffiths J, Martin FJ, Wei Y, Lin HC, Yancopoulos GD, Glass DJ 2005. Insulin-like growth factor-1 (IGF-1) inversely regulates atrophy-induced genes via the phosphatidylinositol 3-kinase/Akt/mammalian target of rapamycin (PI3K/Akt/mTOR) pathway. *J Biol Chem*. 280(4): 2737-44.

Lavasani M, Lu A, Peng H, Cummins J, Huard J 2006. Nerve growth factor improves the muscle regeneration capacity of muscle stem cells in dystrophic muscle. *Hum Gene Ther*. 17(2): 180-92.

Lehto MU, Järvinen MJ 1991. Muscle injuries, their healing process and treatment. *Ann Chir Gynaecol*. 80(2): 102-8.

Levenberg S, Rouwkema J, Macdonald M, Garfein ES, Kohane DS, Darland DC, Marini R, van Blitterswijk CA, Mulligan RC, D'Amore PA, Langer R 2005. Engineering vascularized skeletal muscle tissue. *Nat Biotechnol*. 23(7): 879-84.

Lowe WL Jr, Kummer M, Karpen CW, Wu XD 1991. Regulation of insulin-like growth factor I messenger ribonucleic acid levels by serum in cultured rat fibroblasts. *Endocrinology*. 127(6): 2854-61.

Lowe DA, Lund T, Alway SE 1998. Hypertrophy-stimulated myogenic regulatory factor mRNA increases are attenuated in fast muscle of aged quails. *Am J Physiol*. 275(1 Pt 1): C155-62.

Marsh DR, Criswell DS, Carson JA, Booth FW 1997. Myogenic regulatory factors during regeneration of skeletal muscle in young, adult, and old rats. *J Appl Physiol*. 83(4): 1270-5.

Mauro A. 1961. Satellite cell of skeletal muscle fibers. *J Biophys Biochem Cytol*. 9:493-5.

McKoy, G., W. Ashley, J. Mander, S.Y. Yang, N. Williams, B. Russell, and G. Goldspink. 1999. Expression of insulin growth factor-1 splice variants and structural genes in rabbit skeletal muscle induced by stretch and stimulation. J. Physiol. 516:583–592

Merritt EK, Hammers DW, Tierney M, Suggs LJ, Walters TJ, Farrar RP 2009. Functional assessment of skeletal muscle regeneration utilizing homologous extracellular matrix as scaffolding. *Tissue Eng* Part A. 16(4): 1395-405.

Merritt EK, Cannon MV, Hammers DW, Le LN, Gokhale R, Sarathy A, Song TJ, Tierney MT, Suggs LJ, Walters TJ, Farrar RP 2010. Repair of traumatic skeletal muscle injury with bone-marrow-derived mesenchymal stem cells seeded on extracellular matrix. *Tissue Eng* Part A. 16(9): 2871-81.

Mizuno H, Zuk PA, Zhu M, Lorenz HP, Benhaim P, Hedrick MH 2002. Myogenic differentiation by human processed lipoaspirate cells. *Plast Reconstr Surg*. 109(1): 199-209

Montarras D, Chelly J, Bober E, Arnold H, Ott MO, Gros F, Pinset C 1991. Developmental patterns in the expression of Myf5, MyoD, myogenin, and MRF4 during myogenesis. *New Biol*. 3(6): 592-600.

Moon G du, Christ G, Stitzel JD, Atala A, Yoo JJ (2008) *Tissue Eng* A 14:473–482

Moriwaki Y, Yamamoto T, Higashino K 1999. Enzymes involved in purine metabolism--a review of histochemical localization and functional implications.
Histol Histopathol. 14(4):1321-40.

Mukherjee A, Wilson EM, Rotwein P 2008. Insulin-like growth factor (IGF) binding protein-5 blocks skeletal muscle differentiation by inhibiting IGF actions. *Mol Endocrinol*. 22(1): 206-15.

Musarò A and Rosenthal N 1999. Maturation of the myogenic program is induced by postmitotic expression of insulin-like growth factor I. *Mol Cell Biol*. 19(4): 3115-24.

Musarò A, Giacinti C, Borsellino G, Dobrowolny G, Pelosi L, Cairns L, Ottolenghi S, Cossu G, Bernardi G, Battistini L, Molinaro M, Rosenthal N 2004. Stem cell-mediated muscle regeneration is enhanced by local isoform of insulin-like growth factor 1. *Proc Natl Acad Sci U S A*. 101(5): 1206-10.

Ohanna M, Sobering AK, Lapointe T, Lorenzo L, Praud C, Petroulakis E, Sonenberg N, Kelly PA, Sotiropoulos A, Pende M 2005. Atrophy of S6K1 (-/-) skeletal muscle cells reveals distinct mTOR effectors for cell cycle and size control. *Nat Cell Biol.* 7(3): 286-94.

Oseas R, Yang HH, Baehner RL, Boxer LA.1981. Lactoferrin: a promoter of polymorphonuclear leukocyte adhesiveness. *Blood*. 57(5): 939-45.

Padoin AV, Braga-Silva J, Martins P, Rezende K, Rezende AR, Grechi B, Gehlen D, Machado DC 2008. Sources of processed lipoaspirate cells: influence of donor site on cell concentration. *Plast Reconstr Surg*. 122(2): 614-8.

Pallafacchina G, Calabria E, Serrano AL, Kalhovde JM, Schiaffino S 2002. A protein kinase B-dependent and rapamycin-sensitive pathway controls skeletal muscle growth but not fiber type specification. *Proc Natl Acad Sci U S A*. 99(14): 9213-8

Payne SH Jr, Brushart TM 1997. Neurotization of the rat soleus muscle: a quantitative analysis of reinnervation. *J Hand Surg Am.* 22(4): 640-3.

Péault B, Rudnicki M, Torrente Y, Cossu G, Tremblay JP, Partridge T, Gussoni E, Kunkel LM, Huard J. Stem and progenitor cells in skeletal muscle development, maintenance, and therapy. *Mol Ther*. 15(5): 867-77.

Pettersson P, Cigolini M, Sjöström L, Smith U, Björntorp P 1984. Cells in human adipose tissue developing into adipocytes. *Acta Med Scand.* 215(5): 447-51.

Pittenger MF, Mackay AM, Beck SC, Jaiswal RK, Douglas R, Mosca JD, Moorman MA, Simonetti DW, Craig S, Marshak DR 1999. Multilineage potential of adult human mesenchymal stem cells. *Science*. 284(5411):143-7.

Prockop DJ 2009. Repair of tissues by adult stem/progenitor cells (MSCs): controversies, myths, and changing paradigms. *Mol Ther.* 17(6):939-46.

Quintero AJ, Wright VJ, Fu FH, Huard J 2009. Stem cells for the treatment of skeletal muscle injury. *Clin Sports Med*. 28(1): 1-11.

Rabinovsky ED, Gelir E, Gelir S, Lui H, Kattash M, DeMayo FJ, Shenaq SM, Schwartz RJ 2003. Targeted expression of IGF-1 transgene to skeletal muscle accelerates muscle and motor neuron regeneration. *FASEB* 17(1): 53-5.

Rantanen J, Ranne J, Hurme T, Kalimo H 1995. Denervated segments of injured skeletal muscle fibers are reinnervated by newly formed neuromuscular junctions. *J Neuropathol Exp Neurol*. 54(2): 188-94.

Rescan PY 2001. Regulation and functions of myogenic regulatory factors in lower vertebrates. *Comp Biochem Physiol B Biochem Mol Biol*. 130(1): 1-12.

Rommel C, Bodine SC, Clarke BA, Rossman R, Nunez L, Stitt TN, Yancopoulos GD, Glass DJ 2001. Mediation of IGF-1-induced skeletal myotube hypertrophy by PI(3)K/Akt/mTOR and PI(3)K/Akt/GSK3 pathways. *Nat Cell Biol.* 3(11): 1009-13.

Sacco A, Doyonnas R, LaBarge MA, Hammer MM, Kraft P, Blau HM 2005.
IGF-I increases bone marrow contribution to adult skeletal muscle and enhances the fusion of myelomonocytic precursors. *J Cell Biol*. 171(3): 483-492.

Sacheck JM, Ohtsuka A, McLary SC, Goldberg AL 2004. IGF-I stimulates muscle growth by suppressing protein breakdown and expression of atrophy-related ubiquitin ligases, atrogin-1 and MuRF1. *Am J Physiol Endocrinol Metab*. 287(4): E591-601.

Saito T, Dennis JE, Lennon DP, Young RG, Caplan AI 1995. Myogenic Expression of Mesenchymal Stem Cells within Myotubes of mdx Mice in Vitro and in Vivo. Tissue Eng. Winter; 1(4): 327-43.

Shen W, Li Y, Huard J 2005. Musculoskeletal gene therapy and its potential use in the treatment of complicated musculoskeletal infection. *Infect Dis Clin North Am*. 19(4): 1007-22.

Smith JK, Carden DL, Korthuis RJ 1989. Role of xanthine oxidase in postischemic microvascular injury in skeletal muscle. *Am J Physiol*. 257(6 Pt 2): H1782-9.

Stitt TN, Drujan D, Clarke BA, Panaro F, Timofeyva Y, Kline WO, Gonzalez M, Yancopoulos GD, Glass DJ 2004. The IGF-1/PI3K/Akt pathway prevents expression of muscle atrophy-induced ubiquitin ligases by inhibiting FOXO transcription factors. *Mol Cell.* 14(3):395-403.

Sun D, Martinez CO, Ochoa O, Ruiz-Willhite L, Bonilla JR, Centonze VE, Waite LL, Michalek JE, McManus LM, Shireman PK (2009) *FASEB J* 23:382–395

Tamir Y, Bengal E. 2000. Phosphoinositide 3-kinase induces the transcriptional activity of MEF2 proteins during muscle differentiation. *J Biol Chem.* 275(44): 34424-32

Tedesco FS, Dellavalle A, Diaz-Manera J, Messina G, Cossu G 2010. Repairing skeletal muscle: regenerative potential of skeletal muscle stem cells. *J Clin Invest*. 120(1): 11-9.

Ten Broek RW, Grefte S, Von den Hoff JW. Regulatory factors and cell populations involved in skeletal muscle regeneration. *J Cell Physiol.* 224(1): 7-16.

Tidball JG, Villalta SA 2010. Regulatory interactions between muscle and the immune system during muscle regeneration. *Am J Physiol Regul Integr Comp Physiol.* 298(5): R1173-87.

Tidball JG 2005. Inflammatory processes in muscle injury and repair. Am J Physiol Regul Integr Comp Physiol. 288(2): R345-53.

Tierney MT (unpublished thesis) 2009. The Effect of Peroneal Nerve Relocation on Skeletal Muscle Regeneration within an Extracellular Matrix seeded with Mesenchymal Stem Cell Populations derived from Bone Marrow and Adipose Tissue.

Tille JC, Pepper MS 2002. Mesenchymal cells potentiate vascular endothelial growth factor-induced angiogenesis in vitro. *Exp Cell Res*. 280(2):179-91.

Tokoyuni S 1999. Reactive oxygen species-induced molecular damage and its application in pathology. *Pathol Int*. 49(2): 91-102.

Tu YK, On Tong G, Wu CH, Sananpanich K, Kakinoki R 2008. Soft-tissue injury in orthopaedic trauma. *Injury*. 39 Suppl 4:3-17.

Tureckova J, Wilson EM, Cappalonga JL, Rotwein P 2001. Insulin-like growth factor-mediated muscle differentiation: collaboration between phosphatidylinositol 3-kinase-Akt-signaling pathways and myogenin. *J Biol Chem*. 276(42):39264-70.

Turner NJ, Badylak SF 2011. Regeneration of skeletal muscle. *Cell Tissue Res.*

Wakitani S, Saito T, Caplan AI 1995. Myogenic cells derived from rat bone marrow mesenchymal stem cells exposed to 5-azacytidine. *Muscle Nerve.* 18(12):1417-26.

Walden DL, McCutchan HJ, Enquist EG, Schwappach JR, Shanley PF, Reiss OK, Terada LS, Leff JA, Repine JE 1990. Neutrophils accumulate and contribute to skeletal muscle dysfunction after ischemia-reperfusion. *Am J Physiol*. 259(6 Pt 2): H1809-12.

Walters TJ, Kragh JF, Kauvar DS, Baer DG. 2008. The combined influence of hemorrhage and tourniquet application on the recovery of muscle function in rats. *J Orthop Trauma*. 22(1): 47-51.

Weiss SJ, 1989. Tissue destruction by neutrophils. *N Engl J Med.*9;320(6):365-76.

Wright DG, Gallin JI 1977. A functional differentiation of human neutrophil granules: generation of C5a by a specific (secondary) granule product and inactivation of C5a by azurophil (primary) granule products. *J Immunol*. 119(3): 1068-76.

Xu R, Boudreau A, Bissell MJ 2009. *Cancer Metastasis* Rev 28:167–176.

Zhang G, Hu Q, Braunlin EA, Suggs LJ, Zhang J. Enhancing efficacy of stem cell transplantation to the heart with a PEGylated fibrin biomatrix. *Tissue Eng* Part A. 14(6): 1025-36.

Zhang G, Wang X, Wang Z, Zhang J, Suggs L 2007. A PEGylated fibrin patch for mesenchymal stem cell delivery. *Tissue Eng*. 12(1):9-19.

Zouris JM, Walker GJ, Dye J, Galarneau M 2006. Wounding patterns for U.S. Marines and sailors during Operation Iraqi Freedom, major combat phase. *Mil Med*. 171(3): 246-52.

Zuk PA, Zhu M, Mizuno H, Huang J, Futrell JW, Katz AJ, Benhaim P, Lorenz HP, Hedrick MH 2001. Multilineage cells from human adipose tissue: implications for cell-based therapies. *Tissue Eng*. 7(2): 211-28.

Zuk PA, Zhu M, Ashjian P, De Ugarte DA, Huang JI, Mizuno H, Alfonso ZC, Fraser JK, Benhaim P, Hedrick MH 2002. Human adipose tissue is a source of multipotent stem cells. *Mol Biol Cell*. 13(12): 4279-95.